Wear characteristics of normal compressive crushing rings

Master's thesis in Materials Engineering

Ahmadreza Babaahmadi

DEPARTMENT OF INDUSTRIAL AND MATERIALS SCIENCE

CHALMERS UNIVERSITY OF TECHNOLOGY
Gothenburg, Sweden 2023
www.chalmers.se

Master's thesis 2023

Wear characteristics of normal compressive crushing rings

Ahmadreza Babaahmadi

CHALMERS
UNIVERSITY OF TECHNOLOGY

Department of Industrial and Materials Science
Division of Engineering Materials
Chalmers University of Technology
Gothenburg, Sweden 2023

Wear characteristics of normal compressive crushing rings
AHMADREZA BABAAHMADI

Supervisor:
Emmy Yu Cao, Industrial and Materials Science,
Magnus Evertsson, Comminution Reimagined Sweden AB

Examiner:
Emmy Yu Cao, Industrial and Materials Science

Master's Thesis 2023
Department of Industrial and Materials Science
Chalmers University of Technology
SE-412 96 Gothenburg
Telephone +46 31 772 1000

Cover:

Typeset in LaTeX
Printed by Chalmers Reproservice
Gothenburg, Sweden 2023

Wear characteristics of normal compressive crushing rings
AHMADREZA BABAAHMADI
Department of Industrial and Materials Science
Chalmers University of Technology

Abstract

This thesis examines the wear characteristics of a promising new rock-crushing technology. This novel method employs a normal compressive force to comminute rocks between two rotating rings. To further understand the wear mechanism of these rings and the ring materials response to this type of wear, a variety of ring materials, including Hardox600, two types of sintered Tungsten Carbide (WC)/Cobalt (Co) matrix, identified as X1 and X2 - where X1 has less WC compared to X2 was used. This range of materials enabled a comparative study of wear patterns under the same operating conditions.

The thesis was carried out through a set of surface studies using Scanning Electron Microscopy (SEM), Energy Dispersive X-ray Spectroscopy (EDS), and Backscatter Electron (BE) imaging. These tools were used to closely examine the worn features on the surfaces of the tested materials. These detailed methods provided a clear view of wear patterns, enabling a better understanding of how the ring materials behave during rock crushing.
After a comprehensive analysis of the crushing principle and surface wear, the high stress three-body abrasive wear was identified as the primary wear mode for this application.
In response to this type of wear, the tested materials displayed contrasting material removal mechanisms. Hardox600, being the softest of the materials, primarily experienced cutting (Ploughing) and repeated plastic deformations, evidenced by slivers on the worn surface.

Conversely, the sintered WC materials exhibited completely different post-wear surface topography. For these materials, most material removal was due to WC particle breakage and subsequent dislodging from the matrix. Of the two sintered materials tested, the one with a higher WC content percentage demonstrated superior wear resistance, underscoring the significance of hardness in relation to the hardness of the abrasives. The superior wear can also be explained by the smaller and more uniform WC used in the Sintered X2 compared to X1.
Based on the wear resistance and hardness of the evaluated materials, we conclude that for optimal wear resistance in this wear application, materials should resist plastic deformation, as it leads to severe wear. To control wear, materials should have a hardness that is on par with that of the abrasives to minimize the severity of wear.

Keywords: Crushing- Wear mechanisms- three body abrasive wear- Hardox600- Sintered WC/Co- Surface analysis

Acknowledgements

I would like to express my deepest gratitude to my supervisors, Emmy Yu Cao and Magnus Evertsson, for their continuous guidance, support, and encouragement throughout my thesis journey. Their valuable insights, thoughtful feedback, and unwavering support were absolutely essential for the successful completion of this work, and I am incredibly grateful for the opportunity to learn and grow under their mentorship.

Additionally, I must extend my sincere thanks to Comminution Reimagined Sweden (CRS) for their trust, support, and collaboration in this project. Their constructive feedback, insightful comments, and ongoing support had a significant and positive impact on the quality and depth of this thesis. I am truly thankful for the opportunity to work with such a supportive and innovative team.

Lastly, I cannot express enough thanks to my family for their constant love, support, and encouragement. Their unwavering belief in my abilities, even during the most challenging times, has always been a great source of strength and motivation for me to strive for excellence and continually improve myself.

Ahmadreza Babaahmadi, Gothenburg, Jun 2023

List of Acronyms

Below is the list of acronyms that have been used throughout this thesis listed in alphabetical order:

BE	Backscatter Electron Imaging
CRS	Comminution Reimagined Sweden AB
EDM	Electro-discharged Machining
EDS	Energy Dispersive X-ray Spectroscopy
HC	Hertzian Cone Crack
HPGR	High Pressure Grinding Rolls
HVOF	High-Velocity Oxygen Fuel
L	Lateral crack
MP	Median Half-penny Crack
MMC	Metal Matrix Composites
PSD	Particle Size Distribution
SEM	Scanning Electron Microscopy

Contents

List of Figures

List of Tables

1
Introduction

The process of comminution, a critical component of the rock milling industry, significantly impacts the global environment. It's estimated to consume as much as 4% of the world's electricity, accounting for half of the energy used at mining sites. Moreover, it produces ultrafine waste material that necessitates specific disposal methods in slimes dams [1]. Traditional milling techniques, such as tumbling mills, have been widely used but are known for their high energy inefficiency.
High Pressure Grinding Rolls (HPGR) have been introduced as a more energy-efficient alternative [2], primarily due to their normal crushing component that results in a wear mechanism involving normal compression, as opposed to the other extensively wear mechanisms.

The rock milling industry has been evolving in response to growing demands for more efficient and sustainable processes. As concerns for the environment and resource conservation continue to gain traction, it has become increasingly important for the industry to explore new materials and technologies that can improve energy efficiency and reduce waste generation. HPGR technology offers a promising avenue for achieving these goals, but further research is needed to optimize its performance and material selection.

Although the compressive fracture wear mechanism significantly affects equipment procurement costs, operational expenses, and machine availability, it remains an under-researched field, lacking a standardized testing method. Previous investigations into High-Pressure Grinding Rollers (HPGR) and their wear characteristics provide useful perspectives for this project. However, given the intricate nature of wear phenomena, it is essential to analyze each wear application individually.

Comminution Reimagined Sweden AB (CRS), a company working to improve crushing technology, has developed its own test equipment and procedures for wear investigations.

1.1 Thesis aim and Deliverable

This Master's thesis aims to assist the company in understanding the wear mechanism behind the crushing machine. Three materials were analyzed in the current study: tempered steel, and two variations of sintered tungsten carbide (WC) with a cobalt (Co) binder, each having different WC contents.

The primary goal of this thesis is to better understand the wear mode/modes when subjected to this specific wear during compressive crushing. Utilizing the scientific method to establish hypotheses and test them to understand the materials resistant to normal wear loading, will form the basis of the experimental design.

The development of a reliable and accurate test method for evaluating compressive fracture wear is a crucial step toward understanding the complex interactions between material properties and wear mechanisms. The proposed testing method and equipment will provide a valuable foundation for future investigations in this area, contributing to a more comprehensive understanding of the wear process and guiding the development of improved materials and technologies for rock milling applications.

A thorough investigation of surface topography alterations and microstructure changes after wear testing was conducted using various techniques such as Scanning Electron Microscopy (SEM), Energy Dispersive X-ray spectroscopy (EDX), Backscattered Electrons (BE), and other microscopy methods. It is anticipated that these studies will shed light on the wear behavior of these materials under specific conditions.

This analysis will provide valuable insights into the development of new wear resistant materials and help to inform decision-making in material selection and manufacturing for rock milling equipment.

The deliverables of this Master's thesis include:

- Obtain a wear graph after the experimental wear tests to rank the tested materials
- Explain the wear mode of the machine based on the test work performed for each of the tested materials
- Determine the material removal mechanism(s) for each material
- Identify crucial parameters related to the tribosystem that will affect the wear

1.2 Limitations

The execution of this thesis encountered several limitations, which are listed as follows:

- Wear, by nature, is a complex and unpredictable phenomenon. Even identical wear applications may yield different results under varying environmental and working conditions. Therefore, finding equivalent wear cases for a more in-depth understanding was challenging due to the absence of directly comparable situations, such as the crushing mechanism and crush machine design.

- No reference material was available to benchmark the original states of the materials against their post-wear conditions. This constraint was particularly noticeable in the analysis of micro-hardness.

- The shape and size of the ring made it difficult to monitor wear progression after each run, posing a challenge in tracking the gradual changes on the surface and within the microstructure.

- As the materials tested varied, and each had a different manufacturer, there might be an unseen influence from manufacturing constraints that were not accounted for in the overall analysis.

- Some tests, particularly those involving smaller gaps, required up to 12 hours of testing. This extended duration meant the thesis was restricted to one test(consisting of 6 individual runs) for each material, potentially compromising the validity of the wear values.

2
Theory and Background

Based on the conducted literature review, this chapter aims to explain the basic concepts of how the machines cause abrasive(rock) breakage and the wear principles that are relevant to this application. Understanding these elements is crucial before analyzing the materials after the conducted wear experiment tests.

2.1 Comminution Industry

Comminution is a sub-sector that falls under the broader mineral processing industry. Mineral processing involves the physical and chemical transformation of mineral resources from their raw state into usable products, such as metals, chemicals, or construction materials.
Comminution is a crucial step in the mineral processing industry, which involves the crushing, grinding, and milling of ores to reduce their size and prepare them for further processing. Comminution is critical to the recovery of valuable minerals from ores and is responsible for a significant portion of the energy consumed in mineral processing operations.
Comminution is the biggest individual energy consumer in hard rock mining operations, accounting for a quarter of the total energy used in mining. Thus, even minor enhancements in these circuits can result in substantial energy savings and reductions in greenhouse gas emissions [3].

In the pursuit of reducing energy consumption and carbon emissions within the industrial sector, enhancing comminution equipment efficiency represents a promising strategy. Accomplishing this objective may entail the use of more energy-efficient equipment, optimizing operational conditions, and reducing the size of the particles to be processed.
To further advance this aim, a comprehensive and systematic exploration of alternative comminution methods that offer more environmentally friendly, sustainable, and energy-efficient solutions is required, as opposed to conventional approaches commonly employed in the industry.

2.2 Crushing Principle

There is a limited amount of research available that investigates the mechanisms and behavior of the crushing machine used in this project. Based on the conducted literature review [4, 5, 6, 7], two techniques share high similarities in terms of machine

design, crushing behavior, and principles. HPGR and smooth roll crushers(Can be identified in a more general group of double roll crushers).

In both machines, almost similar to our case, rocks are crushed using mostly compression force and some degree of shear force [6]:

- Compression: When the material is fed between the rolls, it experiences compressive forces, which cause the particles to break.

- Shear forces: The rolls, rotating in opposite directions, create shear forces as they pull the material through the gap. These forces act on the particles, causing them to break along their natural weak points.

As previously noted, the CRS crushing machine exhibits similar crushing mechanisms to both HPGRs and smooth double-roll crushers.
In these machines, the comminution of ores takes place through the application of normal forces as abrasive ores are fed into the gap between two rotating rings. The normal compression force acting within this gap causes the ores to fracture. To ensure the effectiveness of this fracture process, a set of parameters must be meticulously taken into account.

It's important to note that despite some similarities, the crushing mechanisms and machine designs of HPGR and the machine examined in this thesis are significantly different. In HPGR, rocks are subjected to a high degree of pressure between rolls, which is usually facilitated by hydraulic systems. However, in the case of the CRS machine, rocks are compressed solely due to the difference between their original size and the gap distance of the rotating roll, without any application of external pressure.

2.2.1 Particle Grip Condition

Figure 2.1 provides a schematic representation of an HPGR or double-roll crusher, illustrating the corresponding component forces involved. To effectively trap a particle between the rings, the drawing force (F_d) must surpass the ejecting force (F_e). Since the horizontal components of the forces from both rings counteract each other, we only need to consider the vertical components. These vertical forces are mainly derived from compression and friction actions. The ejecting force (F_e) stems from the vertical aspect of the normal force (F_n), which acts as the counterforce at the contact point between the particle and the rings. On the other hand, the drawing force (F_d) originates from the vertical component of the friction force (F_r) [5]. The relationship among these forces is as follows:

$$F_e = F_d.sin(\alpha/2) \tag{2.1}$$

$$F_d = F_r.cos(\alpha/2) \tag{2.2}$$

In above equations α is determined as the gripping angle [5],[8]. As can be under-

stood the particle will be captured by the rings when:

$$F_d \geq F_e \tag{2.3}$$

With having equations 2.1,2.2,2.3 we will have:

$$\mu \geq tan(\alpha/2) \tag{2.4}$$

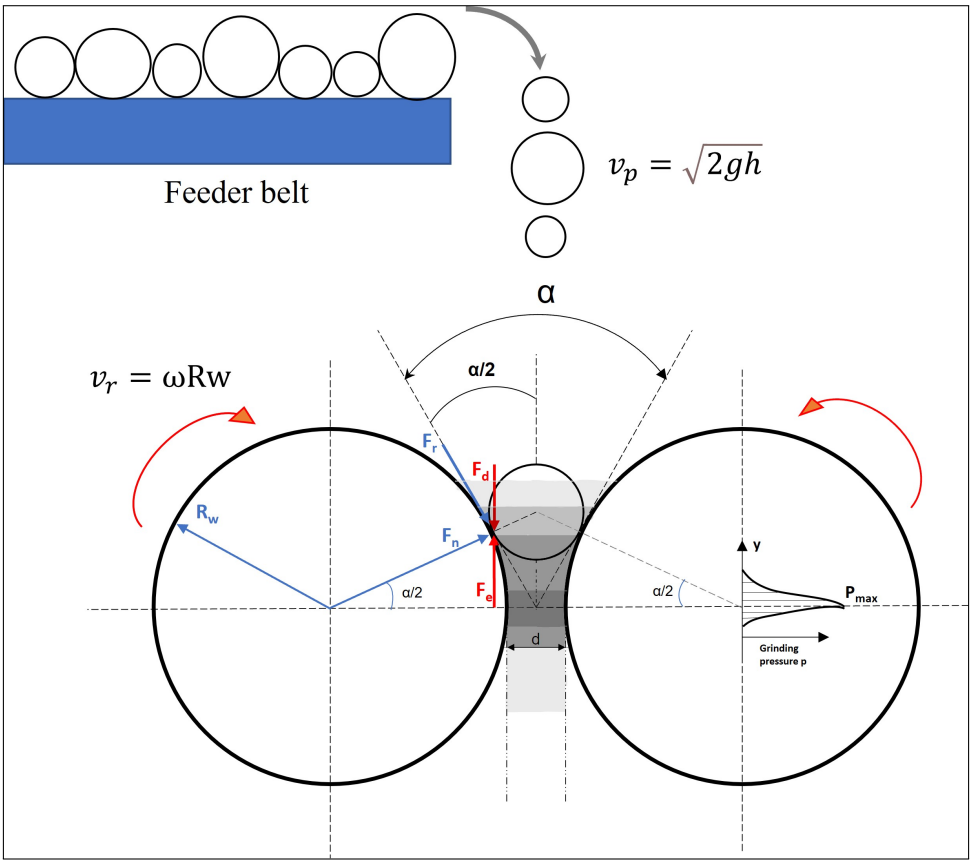

Figure 2.1: Force visualization from the front side of the machine[5],[8],[7]

Generally, friction can manifest in two primary forms: static friction, denoted by the coefficient μ_H, and kinetic friction, represented by μ_G. Static friction arises when a particle touches the roll surface moving at the same speed, facilitating immediate engagement. This situation arises when the circumferential speed vectors (V_r) and the particle speed (V_p) align, which happens exactly along the line connecting the roll rotation centers within the crushing gap. Yet, the crushing process for the particle starts well before this point and is usually finalized by the time the smallest crushing gap is reached. In other scenarios where the particle strikes the roll surface at a differing speed, it slides until its speed aligns with the rolls. Here, the kinetic friction coefficient μ_G becomes essential for accurate computations [5].

2.3 Wear Principle

Wear is a common phenomenon in various industrial and day-to-day situations. The concept of wear involves diverse interpretations when analyzed and anticipated

within various contexts. In most definitions, wear signifies the "loss" or "damage" of material due to the relative motion of a counterpart surface against the material [9, 10, 11]. This intricate process leads to degradation and, ultimately, the gradual removal of material as the contacting surface displaces the subjected material[12]. Addressing a particular wear problem relies on determining the characteristics of the specific wear system involved. Depending on a tribosystem's parameters, diverse wear mechanisms might be present.

The task of predicting and modeling wear presents significant challenges due to several underlying factors. Three primary reasons contribute to this complexity [12]:

- **Transformation of Near-Surface Layer:**During wear, the properties and composition of the near-surface region experience alteration, warranting separate and distinct investigation as an independent material layer. The historical progression and evolution of this layer necessitate separate investigation apart from the material undergoing wear.
- **Dynamic Topographical Changes:** As the material is worn from the surface, it initiates alterations in topography, perpetually influencing the behavior of the tribosystem through continuous modifications.
- **Intricate Wear Mechanisms:** Wear frequently occurs through intricate mechanisms, encompassing a range of mechanical material removal approaches and potential chemical interactions between the surface and external agents, such as lubricants.

Consequently, due to the intricate nature of wear, a definitive empirical correlation that quantitatively links wear quantity with operational factors like load, speed, and material properties has not yet been established. Pursuing a singular relation of this kind is, in fact, somewhat futile due to the diverse and distinct phenomena encompassed by wear.

The absence of a unified empirical wear law has significantly restricted engineers from effectively addressing wear-related challenges during machinery design. Unlike established quantitative relationships like Hook's law for elastic bodies, there isn't an equivalent law that explains wear. This deficiency makes it challenging to apply dimensional analysis for predicting wear in actual machinery based on results from small-scale laboratory tests [13].

Understanding wear rates, and various types of wear mechanisms, are crucial for designing tribosystems and choosing suitable materials according to the material's wear map.
The predominant type of wear in a system can change from one form to another, influenced by surface material characteristics and dynamic surface reactions from friction between the elements in contact.

Wear mechanisms provide insights into the intricate alterations that occur during friction. Typically, wear does not result from a single wear mode, thus, it becomes important to comprehend each individual wear mechanism within a particular wear

application [14].

A wide range of techniques are used for wear testing, and while there is no universal standard specification for such tests, some methods have gained broad acceptance in laboratories globally. The reason for this assortment of testing techniques lies in the multitude of wear systems found in practical applications. Even when employing similar methodologies, test results from different researchers and laboratories can generally only be qualitatively compared due to variations in testing procedures, like test piece dimensions, geometry, environment, and so on. As a result, it is essential to be aware of the exact testing conditions when evaluating test outcomes. The successful application of laboratory test results to real-world industrial scenarios can be expected only when the key parameters of tribosystems in both lab and practical settings are closely aligned [15].

In this section, we will investigate the wear mechanisms relevant to the CRS crushing machine by comparing it with similar crushing machines or crushers used in wear tests. We aim to highlight the similarities and differences in the wear mechanisms to provide a better understanding of the wear behavior in the CRS crushing machine.

2.3.1 Wear Classification

It is crucial to identify the tribosystem when investigating a wear case, as emphasized repeatedly. For conducting this we must identify four important elements listed below [15]:

- The material undergoing wear (Body)
- The second material (Counter body)
- The interfacial region or elements contacting the two bodies
- Environmental conditions

An example of this can be seen in Figure 2.2.

As previously stated, a crucial factor in the identification of a tribosystem involves analyzing the interfacial region between the interacting bodies, along with the subsequent determination of their contact type and configuration. This criterion serves as a valuable tool for categorizing distinct processes, a method that has been employed by Kato and Adachi [17].

With this graph(Figure 2.3), any type of wear application can be categorized into four major modes as Burwell has suggested as well [13]:

- Adhesive wear or galling wear
- Abrasive wear and cutting wear
- Fatigue wear
- Corrosive wear

By categorizing the nature of body interactions and the method of material removal according to the state of deformation, it becomes easier to discern the potential processes leading to material removal and eventual material failure. This organized

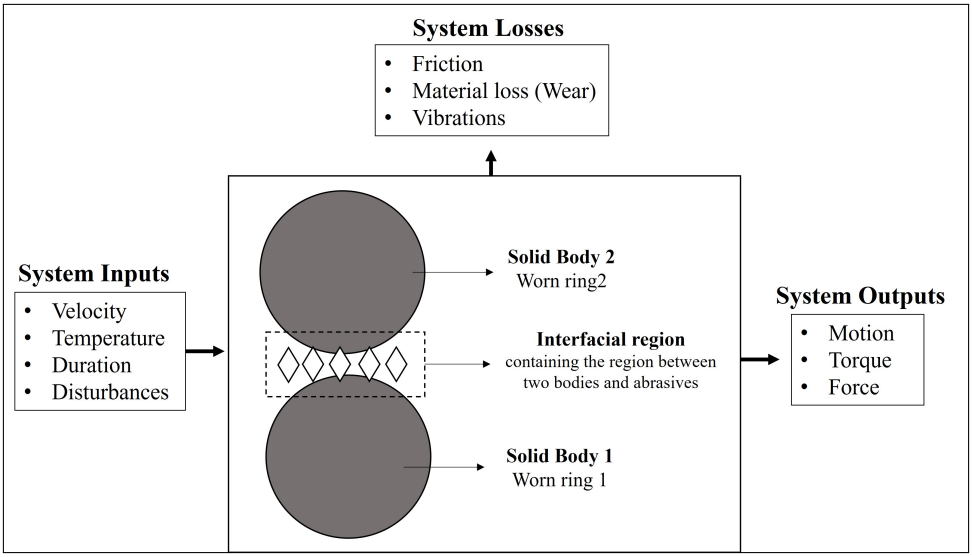

Figure 2.2: An example of a tribosystem with it's important elements [16, 15]

approach facilitates clearer identification for subsequent investigative purposes. By identifying contact types as wear modes we can better understand and differentiate obscure wear mechanisms such as abrasive or fatigue wear.

As explained in the previous section, a significant component of the CRS machine is the presence of ores, which serve as the abrasives to be crushed within the gap between two rotating rings. This particular setup, along with the cyclic interaction between the ring materials and the abrasives during the crushing process, highlights the significance of investigating abrasive wear processes.

In the coming sections abrasive wear as the probable wear mechanism for the CRS machine will be described.

2.4 Abrasive Wear

Given the operational principle of the CRS crushing machine and the characteristics of its tribosystem, it seems intuitive to primarily focus on abrasive wear when exploring the wear mechanism.

Abrasive is a type of wear that occurs due to the contact between a particle and a solid material. It refers to the removal of material from a surface as hard particles pass over it. Abrasive wear involves material loss as hard particles move across the surface. This type of wear occurs when a solid object comes into contact with particles that have equal or greater hardness than the subjected material [15][18].

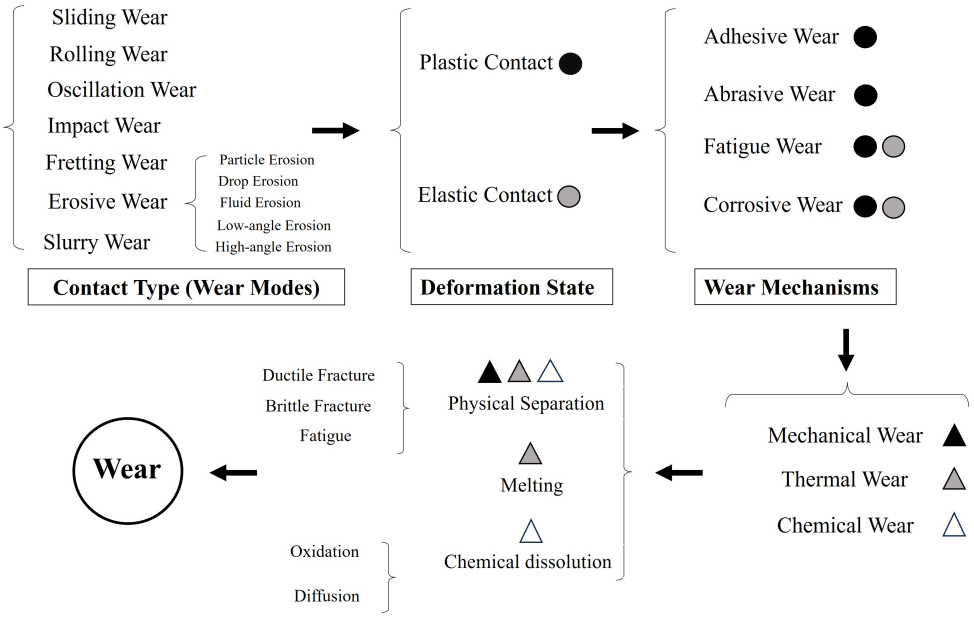

Figure 2.3: Different wear classification with focus on contact type *Modified from [17, 15]*

2.4.1 Abrasive wear classification

The primary abrasive wear mechanism, which significantly impacts mining and mineral processing equipment, can be categorized into four major sub-mechanisms [19]:

- Gouging abrasion
- High stress (Grinding) abrasion
- Low stress (Scratching) abrasion
- Erosion-corrosion

This categorization is primarily based on how the abrasives interact with the worn material's contact surface. It revolves around understanding the nature of contacts, the abrasives' behavior during wear, and, most importantly, the worn material's response when in contact with abrasives.

Gouging abrasion: Gouging happens when large segments of hard abrasive particles press into worn surfaces and slide across them with strong force. This type of wear includes both cutting and tearing actions. Sharp points of rock under pressure cause small pieces of metal to be pulled away from the surface. Gouging abrasion results in the surface becoming plastically changed and harder due to the abrasive impact. The degree of surface deformation that warrants the use of "gouging" term is not clearly demarcated [19],[18].

High stress(Grinding) abrasion: This type of abrasion happens when the abrasive particles fracture during the wear process. How the abrasives during the wear remove surface material is not well known yet. It has been seen that material removal in this type occurs by a combination of different modes like cutting, plastic deformation, fracture, tearing, fatigue, and delamination.

A significant consideration in this classification is the relative hardness between the worn material and the abrasives. When the material and abrasives have similar hardness levels, it prevents the material from undergoing extensive plastic deformation and substantial wear before the abrasives break.[19],[20].

Low stress(Scratching) abrasion: Despite the previous class, this type won't cause breakage of abrasives due to considerably lower stresses during wear. When abrasive particles make lightly loaded contact with the worn surface, low-stress scratching abrasion occurs, which results in microscopic cutting and ploughing. Corrosion can also affect the general wear rate in circumstances involving water or other liquids. The active wear mechanism is known as erosion-corrosion in this case. Low-stress abrasion is the main wear mode in both situations. The wear rates for low-stress abrasion are comparatively low [19].

Table 2.1 is the summary of this classification based on the configuration of contact and environmental conditions [19],[21].

Table 2.1: General abrasive wear classification [19, 21]

Classification	Gauging Abrassion	High-stress Abrasion	Low -stress Abresion	Erosion- Corrosion
Abrasive size	Large	Medium	Small	Fine
Contact Conditions				
Impact	High	Low	Low	Low
Force	High	High	Low	Moderate
Velocity	Low	Low	Variable	High
Impingement angle	Low	Low	Medium- Low	Variable
Environmental	Generally dry	Generally as Slurry , Variable Ph	Variable	Generally as Slurry, Variable Ph
Principle Mechanism	Plowing, Cutting	Cutting, Fragmentation, Corrosion	Cutting, some corrrosion	Cutting, Plowing, Fragmentation, Corrosion

The wear rate for the mentioned mechanisms is influenced by how deeply abrasive particles indent the worn material. The depth of this indentation under specific wear conditions relies on the hardness of the worn material and the attributes of the abrasive particles, including their hardness, shape, and size. Additional information about these abrasive characteristics will be discussed in the upcoming section [19].

There is another way to see the interaction between hard abrasives and the material's surface. Based on that wear can be categorized into two distinct types of wear [22]:

- Two-body abrasive wear
- Three-body abrasive wear

Two-body abrasion takes place when wear is induced by rigid protrusions on the counterface or hard particles adhering to it. On the other hand, three-body abrasion occurs when hard particles move freely, rolling and sliding between distinct sliding surfaces.

From the explanations given for high-stress and low-stress abrasion, it can be understood that three-body abrasion is predominantly associated with high-stress situations, while two-body abrasion is more closely linked to low-stress scenarios. It's important to note, however, that there are instances where two-body abrasion can occur under high-stress conditions as well [19].

The wear process cannot be fully described by simply categorizing it into "two-body" and "three-body" based on whether the particles are fixed or loose. Free particles can either slide or roll in the space between surfaces and in certain situations, they might simultaneously slide in one area and roll in another. As such, it is often more accurate to label abrasion as either sliding or rolling abrasion, in accordance with the motion of the particles.
Consider the instance of a drill cutting through rock, which typically experiences two-body sliding abrasion. On the other hand, grit particles trapped between sliding surfaces, perhaps as impurities in lubricating oil, could either slide or roll - both circumstances are categorized as three-body abrasions.
Generally, the wear rates associated with rolling abrasion are lower than those due to sliding abrasion. However, the methods of material removal in both scenarios might primarily differ in their relative significance [18].

Before exploring the detailed material removal mechanisms linked to abrasive wear, it is beneficial to develop a fundamental understanding of the diverse contact types. This foundational knowledge helps in interpreting how materials react to specific wear mechanisms, such as abrasive wear.

2.4.2 Different contact types

Generally, contacts can be categorized into [23]:

- Elastic contact
- Elastic-plastic contact
- Fully plastic contact
- Brittle contact
- Viscoelastic contact

2.4.2.1 Elastic contact

The contact between two bodies can be classified as either conformal or non-conformal, depending on their geometric arrangement. Conformal contact takes place when the surfaces of two bodies come into complete contact with each other, as seen in scenarios like bearings and shafts. On the other hand, if the contact doesn't encompass this full contact, non-conformal contact happens at a specific point or along a line. For instance, point contact occurs between balls and races in a bearing, while line contact occurs between the teeth of gears [23].

The example below (shown in figure 2.4 a) is from an ideal elastic point contact

for two different bodies. Based on this setting we can have these relations between the corresponding parameters [23], as given in Eq 2.6:

R, E, and ν with their subscripts are the radiuses, Young's modulus, and Poisson's ratios of the two contacted bodies respectively.
With a as the radius of the circular contact region, the apparent contact area of two bodies will be as given in Eq 2.5:

$$A_n = \pi.a^2 \tag{2.5}$$

$$a = (\frac{3.F_N.R'}{2E'})^{1/3} \tag{2.6}$$

F_N is the normal force, R' is the reduced radius of curvature and E' is the effective Young's modules, given by the following Eq 2.7 and 2.8, respectively:

$$\frac{1}{R'} = \frac{1}{R_1} + \frac{1}{R_2} \tag{2.7}$$

$$\frac{1}{E'} = \frac{1}{2}.(\frac{1-{\nu_1}^2}{E_1} + \frac{1-{\nu_2}^2}{E_1}) \tag{2.8}$$

Based on the Hertz theory the contact pressure distribution, as shown in Figure 2.4 b), will have its maximum value at r=o, which is the center of contact(Eq 2.9) :

$$p = -\sigma_z(z=0) = p_{max}.\sqrt{1-\frac{r^2}{a}} \tag{2.9}$$

The Hertzian pressure (maximum pressure) which occurs at the center of contact is given by the following Eq 2.10:

$$p_{max} = \frac{3F_N}{2\pi a^2} \tag{2.10}$$

At the edge of the nominal area of contact, a tensile radial stress occurs. Its maximum value(at r=a) can be determined by following Eq 2.11:

$$\sigma_r = p_{max}\frac{1-2\nu}{3} \tag{2.11}$$

At 45° with respect to the contact surface, maximum shear stress(τ_{max}) will develop. Maximum shear stress distribution can be found by Eq 2.12:

$$\tau_{max} = \frac{1}{2}|\sigma_z - \sigma_r| \tag{2.12}$$

Another important parameter is the occurrence of the shear stress(τ_{yz}), which is normal to the z and y axis and happens due to lateral displaces beneath the contact area (Figure 2.4c).

All the equations mentioned are significant not only for the calculation of stress and pressure within tribosystems but also for analyzing the nature of contact. In

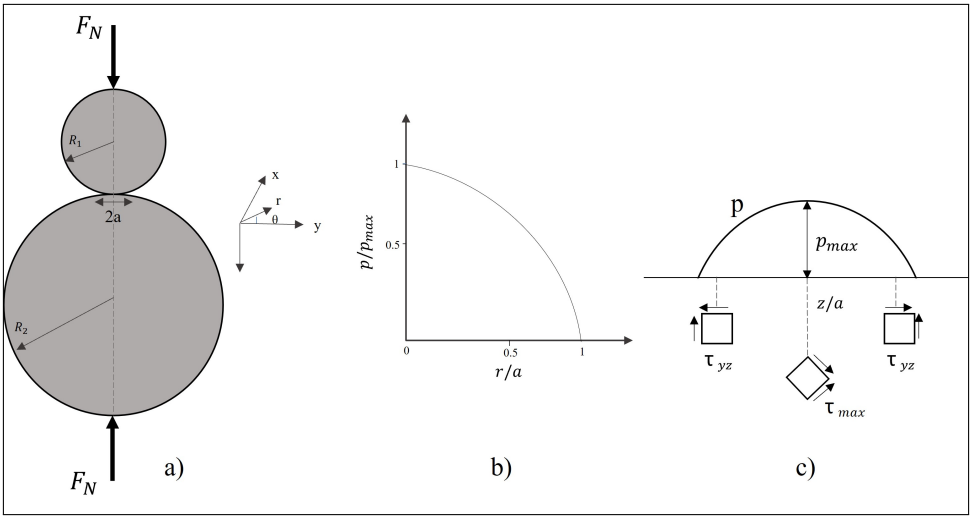

Figure 2.4: An example of a contact point for two spherical bodies
Taken from [23]

practical situations, purely elastic deformations are limited; instead, there is usually some degree of plasticity involved. Hence, it's essential to initially analyze a system in its simplest configuration, characterized by elastic behavior. Subsequently, considering other conditions and criteria, the type of contact can be determined.

2.4.2.2 Elastic-plastic and fully plastic contact

Depending on the material's ductility, the contact area can experience localized plastic deformation. This occurs when stresses reach or surpass the yield strength at a critical point, leading to a shift from purely elastic behavior to a combination of elastic and plastic responses.

In the case of conformal contacts, yielding typically starts at the surface and may extend to the edges. Conversely, non-conformal contacts see yielding initiation at a certain depth, denoted as z_m. According to the Tresca criterion, when $\tau_{max} = \tau_Y$ (Shear yield stress) $= \frac{\sigma_Y}{2}$ happens, the material begins to yield. This yielding results in localized plastic zones beneath the surface. With increasing the load, the plastic zone can expand, if the load is removed and the pressure is below the critical value, the remaining load will cause elastic deformation only. This phenomenon is known as elastic shakedown.

If the load is high enough that expand the plastic zone to the surface, then the contact transfers to the fully plastic. This happens when the nominal pressure (p_0) equals to the critical value(yield pressure p_Y). Yield pressure is greater than the yield stress and it is defined as $p_Y = b\sigma_Y$. b value can be as difficult to spread the plasticity. As can be understood, the b value depends on the geometry, loading conditions, and the characteristics of the material [23].

2.4.2.3 Brittle contact

When the material possesses high yield strength but relatively low fracture toughness, the likelihood of encountering a brittle contact increases. In scenarios characterized by brittleness, the contacting bodies could exhibit micro-cracks on either one or both surfaces. These micro-cracks become subjected to critical stress that leads to their opening or propagation. When the radial stress(σ_r), as introduced in Eq 2.11, exceeds the critical value(σ_F) defined by the following Eq 2.13[23]:

$$\sigma_F = \frac{K_{1C}}{1.12\sqrt{\pi c}} \tag{2.13}$$

In this equation c and k_{1C} are the length of the crack and the fracture toughness of the material, respectively.
During this type of contact, there are some alterations in the material which lead to material loss, as described in the following [24, 25]:

Crack initiation: Cracks in a material often originate from its existing imperfections. This means that the initial cracks, or "crack nuclei," typically emerge from the material's inherent defects(Figure 2.5 a). However, there's another way that cracks can form: during the process when the material is indented or pressed(when deformation is induced). The type of indenter used—whether it's blunt or sharp—determines how these cracks will appear:

- With a blunt indenter, cracks tend to begin at the pre-existing imperfections on the material's surface.
- On the other hand, when using a sharp indenter, cracks are more likely to start from new flaws that develop below the surface due to the deformations during indentation.

Crack formation: When a solid material is subjected to pressure, it can start to develop cracks. These cracks initiate and expand from the most significant imperfection within the material as the force from the indenter is increased. The growth of this crack, particularly in its early stages, is steady and doesn't happen spontaneously (Figure 2.5 b). This is because there exists an energy threshold that the crack must overcome to grow further. This energy barrier can be attributed to certain mechanisms within the material that limit the stress, termed here as "stress cutoffs."

Crack propagation: When the energy needed to start a crack exceeds a certain threshold, the crack rapidly spreads. However, it stabilizes once it reaches a depth beyond its initial point of contact or pressure. At this stabilized stage, the crack is termed "well developed." This means that with increasing the load as the driving force, the deformation-induced zone stably increases.

There are two primary types of such mature cracks:

- The Hertzian cone crack starts from a surface defect and is caused by the pressure of a sphere pressing against the material. When you look at its pattern

of spread (visualized in a referenced figure), it looks like it grows outward in a circular manner, centered around where the initial pressure was applied. This crack grows in a direction perpendicular to the material's surface.

- The median half-penny crack is initiated by the sharp tip of a cone or pyramid-shaped indenter. This type of crack starts from a deformation caused by the pointed pressure. Its growth pattern is also radial and circular but spreads parallel to the surface of the material.

Interestingly, several of these mature cracks can grow either sequentially or even simultaneously, influenced by other physical or chemical forces. This behavior is especially evident when the material is subjected to varied pressures or conditions (Figure 2.5 c).

Unloading crack: When the pressure from the indenter is released, the cone and median cracks tend to close, but not completely (Figure 2.5 d). This unloading process leads to the emergence of residual stresses. These stresses result from the mismatch between areas that were permanently altered due to the indenter's plastic deformation and the adjacent, unchanged elastic regions. This stress discrepancy sets the stage for a new type of crack formation (Figure 2.5 f).

These new cracks, known as 'lateral' cracks, originate from the previously deformed zone and grow both sideways and upward towards the material's surface. The exact mechanics of these lateral cracks remain a bit elusive, primarily because the underlying residual stresses are intricate and not entirely understood. Yet, it's evident that these lateral cracks play a significant role in detaching material from the surface.

The formation and growth of these lateral cracks are closely tied to how intensely the material was deformed. Sharp indenters, which concentrate stress more intensely, are especially influential in this process, accentuating the deformation and, consequently, the development of these lateral cracks.

2.4.2.4 Viscoelastic contact

This form of contact is primarily observed in polymeric materials. In this context, when a load is applied, the material exhibits both elasticity and viscosity.
One noteworthy distinction from other contact types is its time-dependent nature. Unlike other materials, viscoelastic substances rely on time to respond to stress and strain. Meaning, when subjected to an abrupt load or stress, they initially behave like an elastic material. However, over time, they can also exhibit the characteristics of a viscous fluid.
This implies that similar to elastic deformation, viscoelastic deformation can indeed recover, but this recovery happens gradually over a duration of time following the release of the load, rather than instantly[23].

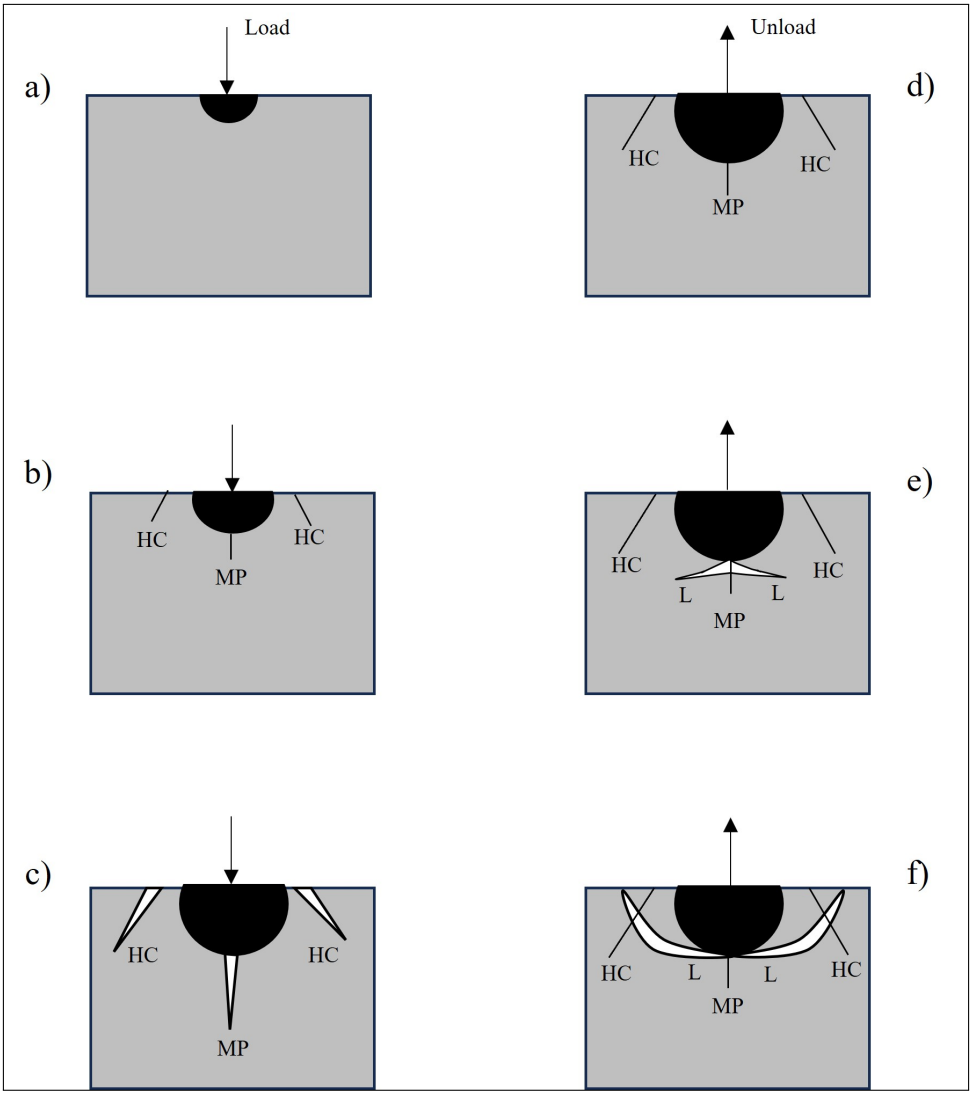

Figure 2.5: Indentation-crack evolution in loading and unloading. (HC) denotes Hertzian cone crack, (MP) denotes Median half-penny crack and (L) lateral crack. *Taken from [24]*

2.4.3 Material removal mechanisms

Abrasive wear can be more extensive than it appears initially. One of the challenges in preventing and controlling abrasive wear is that the term 'abrasive wear' doesn't accurately capture all the wear mechanisms involved. In reality, many wear modes, or to put it another way, material removal mechanisms frequently coexist [22]. Figure 2.6 illustrates some of the probable mechanisms that are associated with abrasive wear.
All of the four: cutting(ploughing), fracture, fatigue, and grain pull-out can be present in an abrasive wear system to some extent based on their material characteristic. An important thing is regardless of the material's hardness or ductility, the material can experience ductile or brittle, and both during the abrasive wear [22],[18].

These different mechanisms can be better understood by considering the contact type which was discussed in the previous section.

2.4.3.1 Cutting

Figure 2.6a, illustrates one of the most well-known mechanisms associated with abrasive wear, where a sharp, hard particle cuts a softer surface. Two primary mechanisms occur in this cutting process: cutting the surface and forming a wedge buildup after the cut, also known as "ploughing" [22]. Depending on the specific wear modes, the formation of wear particles will vary. When the cutting mode is active, the resulting wear patterns often have an elongated and curled appearance, resembling ribbons. This particular type of wear is influenced by minimal friction. These particles form at the tip of the grooving asperity as demonstrated in 2.6a, where they remain and act like built-up wedges, facilitating the continuation of the grooving process [14].

The ploughing mechanism is mostly involved in the plastic contact and deformation of the worn material. Thus, the hardness and toughness of the worn material would be an important factor.

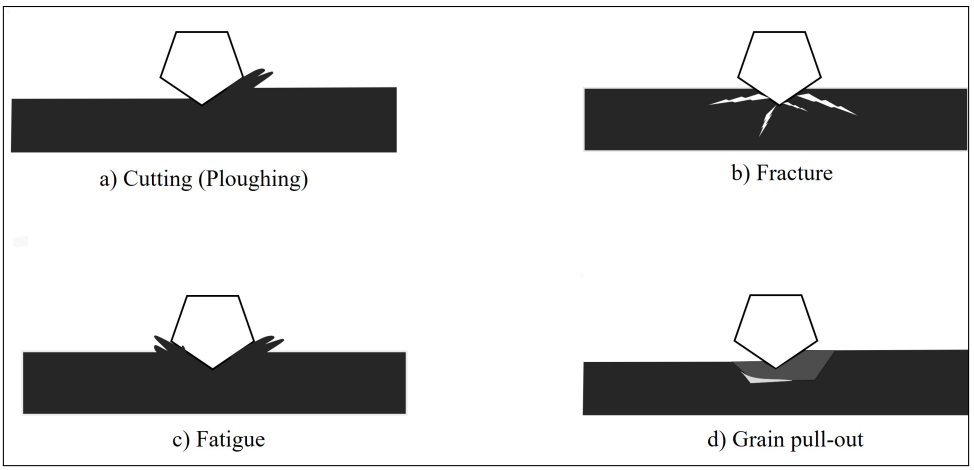

Figure 2.6: Probable material removal mechanisms for abrasive wear [22]

2.4.3.2 Fracture and grain pull out

If the material exhibits brittle behavior upon contact, it will either develop fractures or experience grain pullouts, depending on how it responds to the cracks. The continuous stress from indentations can cause localized fractures, which can escalate into significant fractures and grain pullouts.

2.4.4 Abrasive characteristics

One crucial aspect to examine in a three-body abrasive wear tribosystem is the third body, which is the abrasive particles between two contact surfaces. The character-

istics of these particles, including their hardness, shape, and size, play a significant role in determining the type and rate of wear. This section will explore the impact of these particle attributes on wear.

2.4.4.1 Hardness

One can realize that as the hardness of the abrasive particle increases the overall wear on the corresponding surface will increase as well. Considering the hardness of the surface and abrasive particle as H_s and H_a respectively, It has been found that wear is most sensitive to these hardness values when $H_a/H_s \lesssim 1$. This implies that when abrasive particles are significantly harder than the contact surface, the precise values of these hardness levels are not crucial. This means for situations where the abrasive particles are considerably harder than the contact surface the exact values of this hardness is less important [18].

This behavior can be explained by looking at the interaction between a single grit particle and a flat surface. When $H_a \gtrsim 1,2H_s$ the surface material experiences plastic flow upon surpassing its yield point(Y), substantial plastic deformation occurs on the surface as the average contact pressure reaches roughly 3Y (three times its uniaxial yield stress). The surface's indentation hardness dictates this contact pressure, which is not significantly influenced by the particle's specific shape. If the particle maintains this contact pressure without breakage(deforming), the surface will undergo plastic indentation as the normal load on the particle increases. However, when $H_a \lesssim 1.2H_s$ the particle undergoes flow or breakage before the pressure on the surface reaches 3Y, the surface will experience only a small degree of plastic deformation [18].
This indicates that as long as the material being tested has not undergone plastic deformation, the wear can be managed. Generally, if the mechanism of material removal is more brittle in nature, the severity of abrasive wear will be lower.

2.4.4.2 Shape and Size

The rate of wear is significantly affected by the particle shapes. Particles having sharper edges lead to increased wear compared to those with round edges. Generally with increasing the angularity of the abrasives, the wear will increase. This difference can get up to 10 times higher for angular abrasives compared to round ones [18].

Abrasive wear's intensity is governed by both the shape and size of the abrasives. A notable decrease in wear is evident when the abrasive's size is under 100 micrometers. This correlation between abrasive size and wear isn't specific to a singular process; it's prevalent across various wear methods, including two- and three-body abrasion, erosion, grinding, and metal cutting. While multiple mechanisms may describe this behavior across diverse types of wear, such as erosive or abrasive, one consistent factor emerges: the amplified residual stress beneath the worn surface. This pattern implies that the abrasive size effect might be intricately tied to the material's properties, especially at its surface. Kramer and Demer have observed that the surface layer undergoes greater work-hardening compared to the material's

deeper layers during wear [26].

A compelling explanation for this phenomenon related to size is the "hard (debris) layer" model, as proposed by Kramer and Demer in 1961 [26, 27]. This model assumes that a layer on the surface, roughly 50-100 micrometers thick, experiences more hardening than the underlying material. Hence, smaller abrasive particles, when interacting with the surface, primarily engage with this hardened layer, facing a tougher resistance than the larger particles. These larger abrasives impact and deform the layers beneath the surface-hardened layer, inducing more wear. However, there's a threshold abrasive size, beyond which the impact of the hardened layer becomes insignificant, leading to a plateau in wear rate despite increasing abrasive size.
It should be mentioned that this is not an unexceptional case. Some materials exhibit regions that are softer in the deformed layer than in the bulk material, as observed by Kramer and Fourie in the case of a single crystal of copper[28, 27]. The study on tool steel used for the hot stamping process also revealed that the material near the worn surface exhibited signs of softening [29].
Thus, it's crucial to examine this phenomenon on a case-by-case basis rather than making broad generalizations for all wear scenarios.

3
Materials Background

In this section, an overview of the properties and characteristics of Hardox600 and WC materials embedded within a Cobalt matrix is presented. Given the lack of comprehensive data regarding the manufacturing process of sintered WC rings, the focus in this section is primarily on studying the general characteristics manufacturing procedure of these Metal Matrix Composites (MMC).

3.1 Hardox600

Hardox 600 is a good choice for tasks demanding superior abrasive resistance, due to its impressive hardness level of approximately 600 Brinell [30]. Classified as a medium carbon steel, it contains roughly 0.47% carbon, as illustrated in Table 3.1. The steel undergoes a quenching and tempering process, which transforms it into martensitic steel, tailoring it specifically for extreme abrasive and impact wear situations. While its unique manufacturing process contributes to its distinctive mechanical traits, its chemical composition is equally vital. The table below underscores that Hardox 600 comprises various elements that significantly enhance its hardenability and toughness.

Besides C, this steel also contains elements like chromium (Cr), nickel (Ni), and molybdenum (Mo), each of which contributes specific benefits. For instance, hard carbides can be formed by Cr and Mo. Mn is a austenite stabilizer. Mo retard the austenite-to-ferrite and pearlite transformation. Boron also plays a critical role in enhancing steel properties. It significantly enhances steel hardness by hindering the onset of phase transformations through its segregation on austenite grain boundaries [31, 32].

Based on the unique properties in hardness, strength, and toughness Hardox600 can be used in versatile applications of the mining, transport, and construction industries.

Table 3.1: Hardox600 Chemical composition[30]

Hardox 600 Chemical Elements (Max%)									
Product Type	C	Si	Mn	P	S	Cr	Ni	Mo	B
Plate	0.47	0.7	1.5	0.0015	0.010	1.2	0.7	0.7	0.005

3.2 Sintered WC/Co

Cemented carbides, commonly known as hard metals or cermets, are composite materials designed to combine the hardness of ceramics with enhanced fracture toughness. These materials are crafted by sintering a blend of metal carbides. Tungsten carbide, with a hardness ranging from 1900 to 2100 HV, is the most prevalent carbide used, typically set within a cobalt matrix. However, variations with other carbides, like TiC and TaC, known as ternary carbides, are also available. During the sintering process, the metal powder(3–30% of the mix) melts and forms a liquid film around the carbide particles, facilitating their bonding (sintering). This results in a composite characterized by remarkable hardness, stiffness, and a fracture toughness significantly greater than most advanced ceramics. The metallic binder, or the softer phase, plays a crucial role in this, as it hinders the initiation and growth of cracks [33] [18].

Cemented carbides are recognized for their remarkable hardness, boasting an elastic modulus three times greater than steel and exhibiting high density. Their hardness values range between 800 and 2000 HV [33] [18]. Notably, when the metallic binder content increases, the fracture toughness gets better, but it diminishes the hardness. The carbide grain size, which typically ranges from 1 to 6 m, is essential in determining their attributes. There are also finer grain sizes in use, such as submicron (0.5–0.8μm), ultrafine (0.2–0.5μm), and nanopowders (<0.2 μm).
Generally, a smaller grain size enhances hardness without negatively affecting fracture toughness [33].

Carbides are highly resistant to sliding and abrasive wear, even at high temperatures, making them ideal for machining tools, sliding bearings, seals, and other wear-prone components. However, they come with drawbacks like limited formability and increased cost. To overcome these, powder metallurgy is used to create near-perfect shaped components. Machining techniques, such as electro-discharged machining (EDM) and grinding, are also utilized. Furthermore, the High-velocity oxygen fuel(HVOF) method allows cemented carbides to be used as surface coatings [33].

3.2.1 Manufacturing process

The production of sintered WC/Co involves two main steps: first, creating the elemental powders, and then sintering these powders to form the solid material. In this section, key parameters involved in the manufacturing process are highlighted. The primary reference utilized is the esteemed book, "Cemented Tungsten Carbides: Production, Properties, and Testing" [34].

3.2.1.1 Powder manufacturing

To produce WC/Co, it's essential to understand the creation process of each individual powder component. In the following section, we'll provide a concise overview of this process.

Tungsten Powder: WC-Co hard metals are mainly composed of Tungsten monocarbide (WC), obtained from carburizing tungsten, which is produced by reducing WO with hydrogen. Tungsten is primarily sourced from minerals like Scheelite (CaWO) and Wolframite ((Fe,Mn)WO). Due to its high melting point, tungsten is extracted using hydro processes. The extraction process, starting from ore concentrate, aims to produce an intermediate compound, often tungstic acid or ammonium paratungstate. Before refining, the ore is pretreated to remove impurities. It's then decomposed to isolate tungsten, forming a compound that undergoes further purification. The final step, turning this compound into metallic tungsten, requires little purification compared to other metals [35].

Cobalt powder: Cobalt, a crucial metal binder in WC-based cemented carbides, is typically found alongside other metals in the earth's crust. The primary sources for cobalt extraction include sulphides, arsenides, oxides, and hydroxides. Historically, cobalt powder was produced by reducing cobalt oxide with hydrogen. Modern cemented carbide industries, however, rely on ultra-fine cobalt powders, which are created through the pyrolysis of cobalt salts, like cobalt oxalate. This salt is derived from the reaction between oxalic acid and cobalt chloride. These powders, initially around 2 μm in size, become even finer during milling with carbide, partly due to a phase change in the cobalt's crystal structure. Milling further reduces the size, ensuring thorough mixing and coating of tungsten carbide particles. A novel method, termed 'Polyol Cobalt,' has been introduced, utilizing the reduction of cobaltous hydroxide with specific glycols. This process yields micron-sized cobalt particles with a narrow size distribution. Notably, while nickel is reduced alongside cobalt, other impurities like Ca, Na, and S are excluded in polyol cobalt [35].

Tungsten carbide: Once the tungsten powder is ready, it's mixed with carbon black and heated to temperatures between 1400-1800°C. The resulting WC grain size usually falls between 0.8-7.0μm, optimized for the final sintered hard metal product. Each mixture batch is standardized for consistency, with both grain size and carbon content being key parameters. While the carburizing temperature can influence grain size, it's vital to maintain exact carbon levels. Insufficient carbon can lead to the formation of a brittle 'eta' phase, while a high amount of carbon produces weakening graphite flakes. Therefore, for optimal hard metal properties, the carbon content must be strictly controlled.

High-quality carbon black used in hard metal production should have low ash (typically 0.1%, indicating impurity levels) and sulphur content, with the latter ideally being below 0.01% due to its significant impact on tungsten carbide grain size. The mixing method of tungsten and carbon black can influence the carbide's grain size.

While the mixing method is less crucial for individual or mechanically aggregated tungsten particles, it becomes vital if the metal contains a firmly bonded polycrystalline structure of the original primary tungsten compound used in refining processes. Effective mixing can produce uniform carbide grains, but if the original structures aren't adequately broken down, it results in larger tungsten carbide particles during carburization, affecting the desired grain size [35].

Carburization Tungsten monocarbide (WC) is primarily produced by carburizing tungsten powder with carbon black. This process requires a specific carbon gas environment, especially in a graphite tube furnace where carbide formation is optimized using carbon under hydrogen. An alternative method uses a high-frequency induction furnace, where the carbon-tungsten mixture is rapidly heated. During carburization, the grain size of the resulting carbide is influenced by factors like temperature and the initial grain size of the tungsten. Notably, finer tungsten powders transform differently into carbide compared to coarser ones. The carburizing temperature plays a pivotal role in determining the properties of the final tungsten carbide. Impurities introduced during the process, especially from carbon sources like lamp black, can affect the grain growth and overall quality of the carbide. The purity of the initial tungsten metal also impacts grain growth, with purer tungsten leading to more significant WC grain growth. This is because the formation of monoatomic layers of impurities at the interfaces and grain boundaries alters the rate of diffusion. Some foreign elements can either reduce or enhance this grain growth, depending on their nature.

Carburizing fine tungsten powder at lower temperatures (around 1300°) leads to a loose agglomeration of WC grains, reducing the risk of local grain growth during WC-Co sintering. The resulting tungsten carbide's grain size mirrors that of the original tungsten, and these disturbed WC crystals enhance reactivity during sintering. In contrast, carburizing at higher temperatures (around 1600°) causes strong agglomeration, increasing the risk of local grain growth and producing larger WC grains with reduced sintering reactivity. For tungsten powder larger than 2.5μm, carburization transforms the original single crystal into a polycrystalline tungsten carbide particle.

During production, various factors can affect the size of single crystal domains in WC particles, with temperature being the most crucial. Higher temperatures enhance carbon diffusion, leading to larger single crystal domains. These domains, rather than WC particle size, determine the microstructure of sintered WC-Co hardmetals[35].

3.2.1.2 Consolidation and sintering:

To produce a fully sintered WC/Co, several steps are required after the initial powder creation. These steps include milling, pressing, dewaxing (or presintering), sintering, and post-sintering operations. A brief overview of each step is provided [36]:

- **Milling**: The carbides and metal binder powders are mixed together. The final product's mechanical properties are significantly influenced by the uniform distribution of cobalt, which is achieved during this milling process. Moreover, milling produces new active surfaces and enhances the defect structures in both carbides and the metal binder. These freshly formed surfaces are highly reactive to gases in the surroundings.

- **Granulation**: After milling, the carbide slurry dries into a very fine powder that doesn't flow easily and has a low density. This makes pressing challenging because of the friction between the fine particles. To overcome this, the powder is granulated, forming loosely-bound clusters. These granulated clusters are generally coarser and rounder, improving flow and making the pressing step more efficient and quicker. Various granulation techniques include compression, rotation, spray drying, and vacuum drying, each offering its own advantages and disadvantages.

- **Green consolidation**: Green compacts are formed by pressing powder with an external force, usually in the range of 21-42 kg/mm^2, to achieve aspecific shape and maintain dimensions. These compacts typically reach around 60% of their potential density. While hard metal components can be almost fully densified during liquid phase sintering, starting with a denser green compact minimizes shrinkage and post-sintering grinding. Double-acting presses, which offer more consistent density distribution, are preferred over single-acting ones. For the compaction process, both hydraulic (ideal for larger parts) and mechanical presses are used. Occasionally, isostatic pressing is chosen for its even pressure application, especially beneficial for bigger components or when aiming to minimize pressure loss. For components like drills and reamers, which have a significant length-to-diameter ratio, extrusion is a favored method.

- **Dewaxing and presintering**: During hardmetal manufacturing, paraffin wax is mixed with the powder to ease the pressing process and protect the material from damage during handling. Once the pressing is done, the wax, now redundant, is removed by heating, either in a hydrogen atmosphere or in a vacuum. It's vital that this removal process doesn't compromise the integrity of the compacted material. The industry predominantly uses fully refined waxes, comprised of compounds like normal paraffins and isoparaffins. These waxes melt between 40-50°C. The process of wax elimination starts at about 150°C, but to thoroughly remove it, temperatures between 250-300°C are necessary. Notably, in environments like hydrogen, the wax remains stable and doesn't break down until temperatures exceed 400°C.

  During the production of hardmetals, components are first shaped and then undergo a final sintering process. These components are initially pressed into basic forms, such as rectangles or circles, and are later refined using techniques like turning, drilling, and grinding. It's important to account for an anticipated shrinkage of approximately 20-25% during the final sintering.

To prevent breakage during the shaping process, the components are presintered at temperatures ranging from 750-1000°C, enhancing their strength. This presintering step can be intricate due to the fine quality of the powder, potentially causing changes in its composition.

- **Sintering**: In the WC-Co composition, a unique liquid known as eutectic forms at 1320°C. The common sintering temperature for the popular hardmetal variant, WC-10 Co, is set at 1400°C. At this temperature level, around 15% of the mixture turns into a liquid phase, where WC blends into cobalt. As the temperature drops, WC particles start to solidify, causing the grains to grow larger. Interestingly, no eutectic structure emerges during the sintering process. When the liquid phase becomes solid, it retains 20-25% of WC, but this percentage decreases as the temperature goes down.
  Sintering WC-Co hard metals involves a series of transformations. Even at subdued temperatures, cobalt either envelops or seeps into the carbide particles. As the heat intensifies, cobalt starts dissolving the carbide surfaces nearby. This action paves the way for WC particles to rearrange more closely, leading to a noticeable contraction in size, especially between 800°C and 1250°C.

Several key variables can significantly affect the sintering process, including the sintering atmosphere, the temperature and duration of sintering, the rates of heating and cooling, and the presence of impurities.

To provide a summarized overview of the consolidation phase in the manufacturing of WC/Co, we can refer to the flowchart 3.1, which highlights the key aspects of each step.

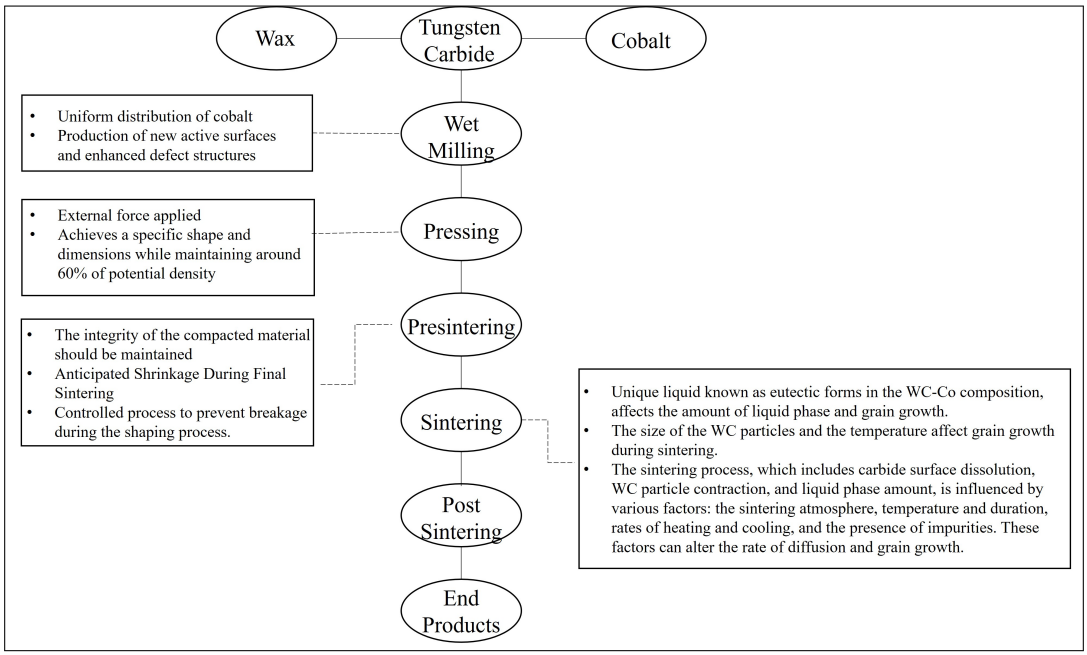

Figure 3.1: Consolidation flowchart of WC/Co
Modified from [36]

4

Test Procedure and Methods

For measuring and investigating the wear, a laboratory-scale crusher machine has been employed. This crushing apparatus operates by a unique technique that exclusively uses normal force for crushing the ores. The figure below 4.1 illustrates the front view of this machine. Two test rings are mounted to a shaft by means of a clamping system. Each of the rings slides onto a split inner ring, which is bolted to a conical shaft. When tightening the screws, the inner ring expands and grips the outer test ring. The test rings have an outer diameter of 125 mm and 30mm width. The gap between the shafts is adjustable. By means of this, the gap between the rolls can be changed for different tests.

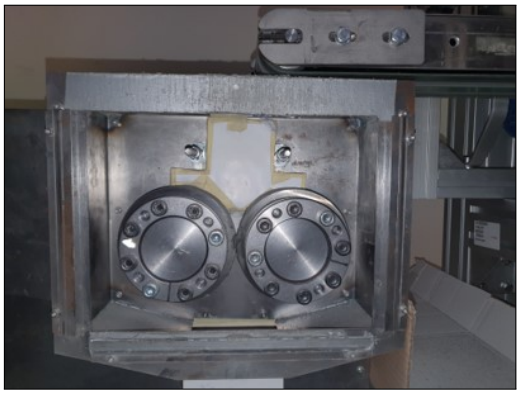

(a) Front view of the rings

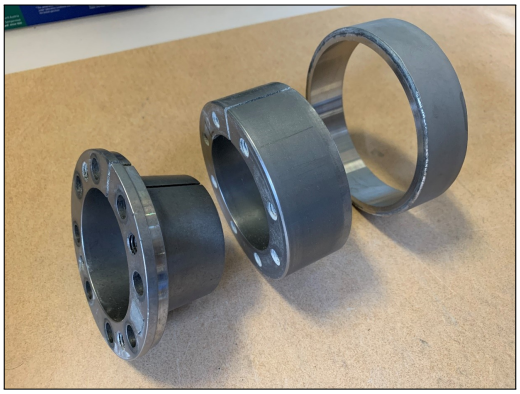

(b) Clamping system of the rings

Figure 4.1: Overview of the rings

Feed material will be directed to the rings using a feed system. The feed system consists of a hopper, an adjustable discharge gate, and a controllable belt feeder. Using adjustment screws more control on the feed has been achieved which is crucial for attaining an optimal falling angle and grip between the rings and the feed material.
Materials pass through an adjustable gate and with a feed belt pores down to the spinning rings. Depending on the test gate height, belt speed and gap between the rolls will change. Further details on these factors will be provided in subsequent sections.

4.1 Test Procedure

The test procedure will be explained in two different sections of wear experiments when wear is introduced to the material and then post-wear tests that have been conducted to understand the characteristics of wear by exploring the material's surface and microstructure.

4.1.1 Wear Experiment

As mentioned in the previous sections the mechanism behind breaking the ores is based on compression and using a normal force to all the ores passing the gap between the rolls. This compression force is accommodated by having gap distances smaller than the feed particle size.

The primary factor in the present wear process is the loss reduction of rings after processing a predetermined quantity of ore in the testing apparatus. It's important to clarify that while measuring the reduction in volume of the rings might be a more accurate way to measure wear for this application, the lack of specific density information for each material made it necessary to use mass loss as the measurement instead of volume loss.

Wear assessment will be conducted through a sequence of tests, involving the alteration of the gap between the rings. In each test, the particle size of the feed material will exceed the gap between the rings. This discrepancy in reduction causes the particles to undergo compression and eventually break down. Wear evaluation is carried out by performing a series of progressively smaller gaps, using the product generated from the prior test as the feed material for the subsequent test, which features a reduced gap. This method ensures a thorough examination of wear under various conditions and contributes to a comprehensive understanding of the wear mechanism.

Additionally, considering the various materials being evaluated for wear, differences in wear properties necessitate an appropriate volume of feed material to effectively discern the distinctions among them. This ensures a comprehensive assessment of the wear performance of each material under the test.

The ring gap is precisely set using feeler gauges. However, difficulties arise due to the rings being somewhat out of round and the mounting surface having similar irregularities. This can result in a deviation as the rings rotate. Furthermore, a skewness between the rings can create a difference in the gap at one end of the ring compared to the other.

During wear evaluations, the feed rate is maintained to ensure that particles enter the rolls in a single layer such that particles are crushed independently. The rings' rotation speed is set to coincide with the falling particles' speed. Previous experiments determined this to be approximately 200 rpm, which is used for all tests.

Fines accumulate in a cyclone, but the wear apparatus's air system is designed solely to minimize dust escape, not to extract the final product.

The feed hopper is filled with the entire test sample, and the feed rate is set to provide the appropriate feed rate to the rings for the specific gap. The data logger is activated, and the test commences, with samples collected randomly throughout the test. A remote control and test stop system allows the equipment to be stopped remotely, as tests can take up to 12 hours for the finest feed. The flowchart of the test procedure can be seen in the figure below 4.2.

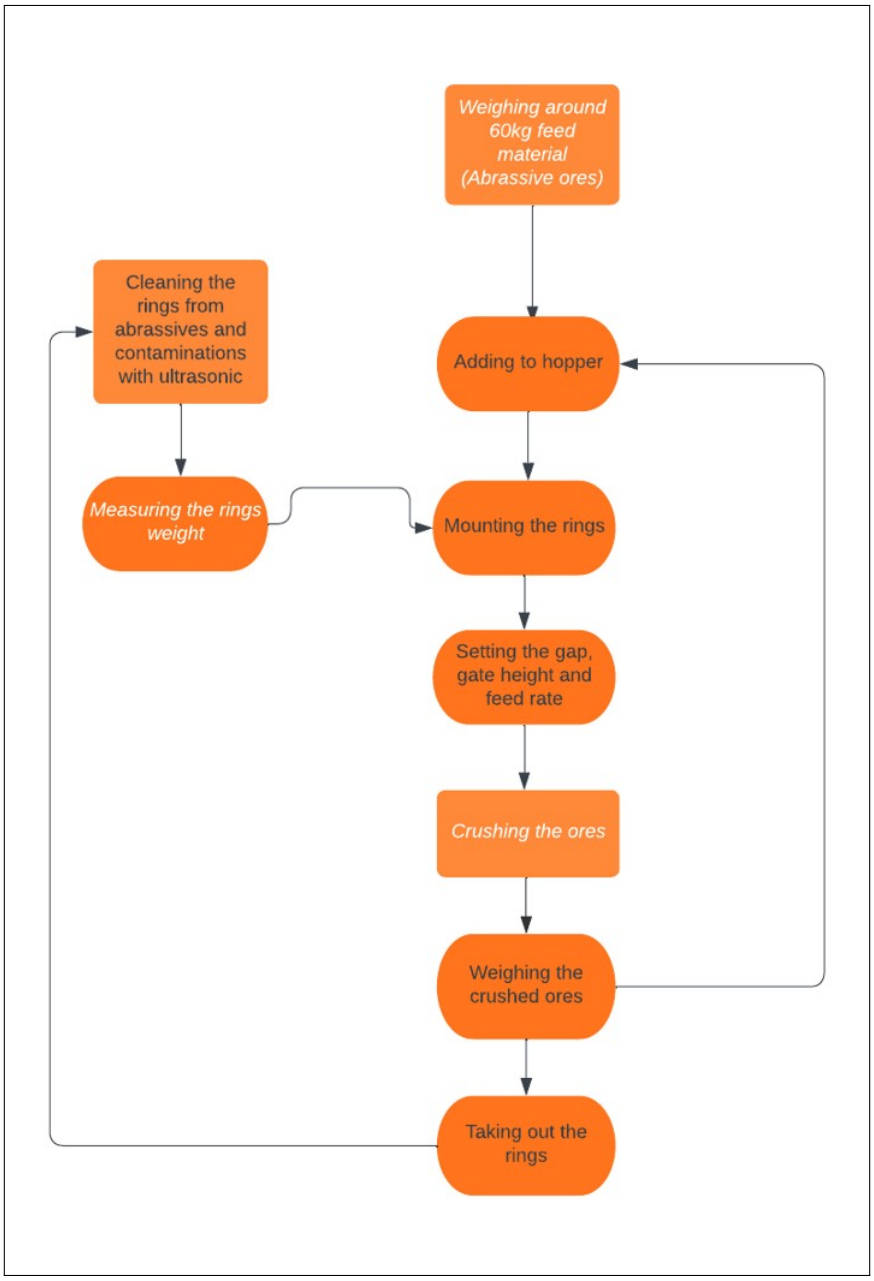

Figure 4.2: Wear experiment procedure flowchart

Following the test, the rings are removed, cleaned in an ultrasonic bath, dried, and then weighed. The feed and product samples are sized to evaluate the reduction extent.

To perform a representative and reproducible wear analysis on various materials, a consistent test plan is implemented to measure wear for tested materials.
Each test consists of six individual tests. For having consistent and similar conditions in all tests, a compression of 0.8 has been chosen for the tests. Compression 0.8 means that first the feed material(ores), with a particle size of 1mm, will be discharged and crushed with a gap distance between rings that is set to 0.8 mm. This is considered as the first run of a whole complete test. The rings after this test will be weighed.

4.1.2 Sample Preparation

To study the wear behavior, each test was followed by a thorough examination of the samples. After the wear tests were completed, the rings were cut to gather two types of samples. The first type of sample was used to investigate the characteristics and topography of the worn surface, providing insights into how the wear process affected the material surface. The second type of sample was consisted of cross-sectional cuts from the rings, which were used to examine the microstructure of the tested materials and understand how the wear process may influence(or be influenced) by the internal structure. A schematic illustration of the samples taken for analysis can be seen in Figure4.3. The samples for microstructure analysis on the cross-section were grinded, polished, and then etched. The etchant used was, Nital, and Murakami's reagent for the sintered WC/Co, as recommended in the literature [37].

4.1.3 Surface Analysis

Due to the size and shape of the rings, observation of the wear surface after each test was limited. After completion of each test, the surface and cross-sectional features were examined for the tested rings. SEM, EDX, and BE were used. Optical and stereo microscopy were also performed for a more detailed examination of the samples.

To monitor the topographic changes of the surface during the wear tests, a stereo microscope was used before the start of each test, in the third run, and in the last run. This approach helped to better understand the surface changes throughout the testing process, which allowed for a comprehensive analysis of the wear behavior of the materials.
To ensure a more reliable analysis, it was tried to examine the same area after each test. This was particularly important for the Stereo Microscope tests, which were designed to monitor the progression of wear for each material throughout the tests This information is essential for the development of improved wear-resistant mate-

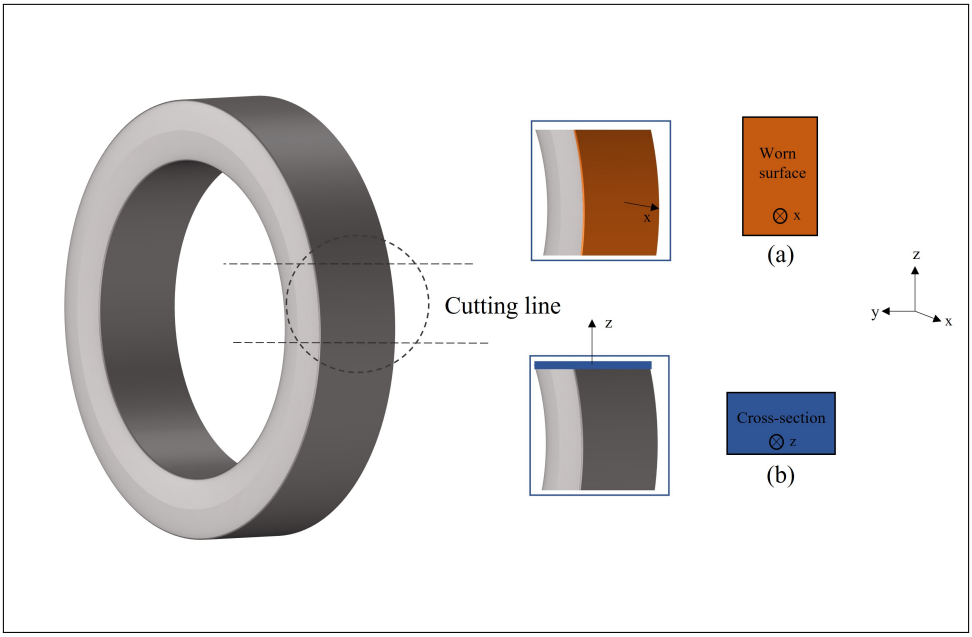

Figure 4.3: Schematic of two different samples taken from rings: a)from the worn top surface of the ring b)from a cross-section of the ring

rials and coatings, and the selection of suitable materials considering manufacturing and application constraints.

4.1.4 Micro-hardness

The micro-hardness test was carried out on all the materials tested in this study. The purpose of this test was two-fold: firstly, to compare the hardness values of the tested materials and secondly, to create a hardness profile across the thickness of the tested rings on the cross-section(refer to Figure 4.3). The hardness profile was obtained by making indentations across the width of the cross-section samples. The indentations were positioned depending on the thickness of the rings, with each indentation being 0.7mm apart from the next. All tests used the Vickers hardness testing method with a load of 5kg (HV5). To ensure the reliability of the tests, several rows of indentations were applied. The average values derived from these multiple indentations were then used to generate the overall hardness profiles.

4.2 Test Plan

To achieve a representative and reproducible wear analysis across various materials, a systematic test plan has been implemented to measure wear for the materials being tested. This plan consists of six distinct tests for each material, ensuring comprehensive investigation and analysis.

A consistent compression ratio of 0.8 is employed for all tests to maintain uniformity in test conditions. This compression ratio facilitates six individual runs within

a complete test, an optimal number for thorough material examination. With a 0.8 compression ratio, the feed material with a particle size of 1 mm is initially subjected to a gap distance of 0.8 mm between rings, signifying the first run of a complete test. In subsequent tests, the gap is reduced by a fraction of 0.8, resulting in tests conducted at 0.8, 0.64, 0.51, 0.41, 0.33, and 0.26 mm gap distances between rings.

The tests commence with approximately 60 kg of feed material, which is considered an appropriate weight for several reasons. It allows for a reasonable timeframe for each test to be completed and enables the wear differences among the various materials to be clearly observed.

The tests consistently used "Quarry rock" as the feed material. While it's challenging to specify the exact composition for each test, it is known that over a third of the material is Quartz, a notably hard mineral. References indicate that the equivalent Vickers hardness of quartz ranges between 750-1200 HV [38, 18].

During each test, random samples were collected from the crushed rocks to examine their particle size distribution (PSD). Analyzing the PSD not only provided insights into the specific patterns of particle sizes for each run, but also helped us gain a better understanding of the machine's crushing accuracy and consistency between each trial. Additionally, this analysis allowed us to identify any potential areas for improvement or optimization, ensuring that the machine operates at its highest level of efficiency when processing rocks. All of the PSD graphs can be find in Appendix C.

As discussed earlier three different types of materials are used for the wear investigation.

Hardened Steel:

- Hardox 600

Sintered WC/Co with different WC percentages

- Sintered X1, with 60% WC
- Sintered X2, with 90% WC

5
Results

The results from the experimental tests and post-wear analysis of each material will be introduced in this chapter.

5.1 Wear experimental results

After carrying out the experiments according to the plan detailed in prior sections, the wear findings for the rings that were tested are provided and illustrated in the figure 5.1.

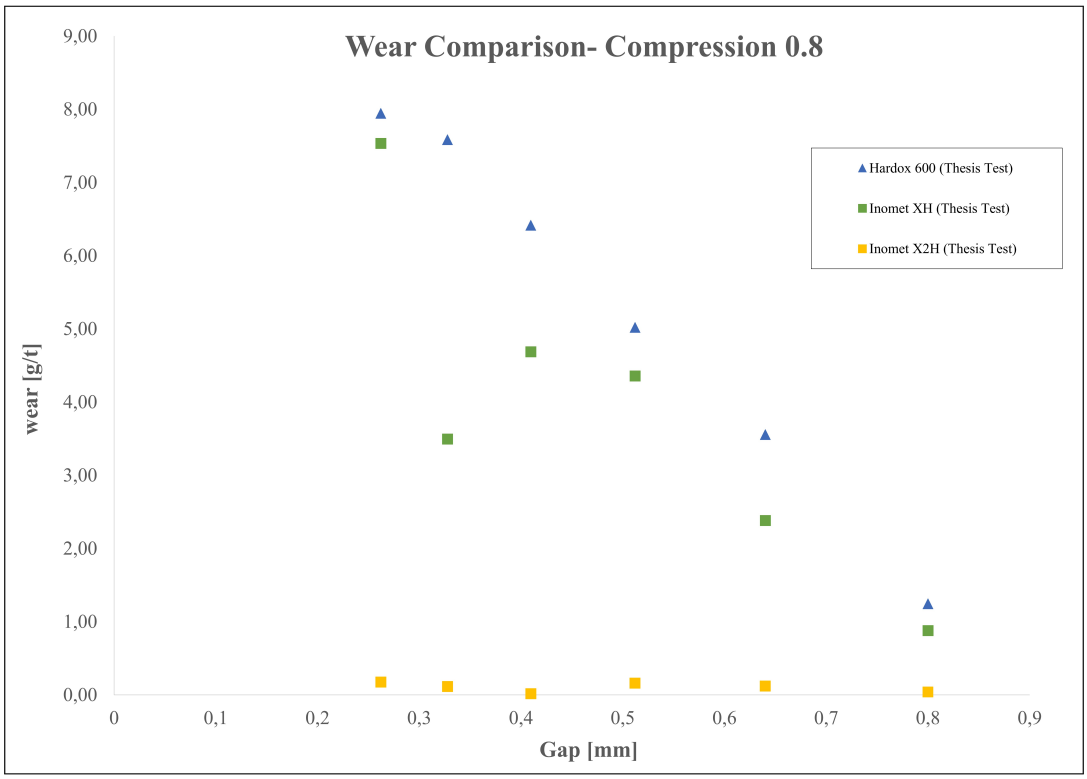

Figure 5.1: Comparison of wear between different tested materials

Examining the wear results, we observe that wear increases for all materials as testing progresses with reducing the gaps. This rise is expected since more number of individual rocks need to be crushed, leading to greater wear on the rings being tested after each run. The wear growth pattern predominantly follows an exponential trend rather than a linear one. However, an exception to this observation is the

Sintered X2, which exhibits an almost linear trend, but with a significantly lower rate of wear compared to the other materials tested.
This observation highlights the importance of understanding wear behavior throughout testing, particularly during the final stages, for accurate crushing machine evaluation.
The graph reveals that the wear rate does not consistently increase between two consecutive individual runs; instead, there are instances where the wear rate decreases before increasing again. This pattern is particularly noticeable in the sintered rings, and it would be intriguing to investigate the cause of this behavior.

It's important to consider that by reducing the gap in each run, more rock particles must be crushed by the rotating rings, even though the total surface area of the rings involved in crushing remains similar in each test. In simpler terms, as the gap between the rolls decreases, the rock size decreases as well, meaning more particles come into contact with the ring's surface. This could be one reason for the exponential growth of wear during a test. As we explore more details about the wear mechanism in the following sections, this trend will become clearer.

According to the findings, the wear resistance ranks from highest to lowest as follows: sintered X2, sintered X1, and Hardox 600. Sintered X2 demonstrates the highest wear resistance among the tested materials.

Various factors could explain the differences in wear resistance among the materials. These factors may include the composition of the materials, their microstructure, the methods used to create them, and their hardness. Another key aspect to consider is the wear mechanism and how each material behaves (the type of wear and the process behind material removal) under this specific wear condition. In this chapter, each material will be analyzed in terms of the factors mentioned, and then compared with one another to have a better understanding of this specific wear.

5.2 Characterization of Hardox 600

Hardox600 was the first material tested for surface examination. Using SEM, EDX, and Stereo microscopy helped track wear progress during the tests, giving a clearer understanding of how material was removed. These findings will be introduced in the following sections.

5.2.0.1 Microstructure

After completion of the wear test, the ring was cut and a cross-section was prepared for the microstructural analysis. For the etching Nital was used. Being a quenched and tempered steel, the expected microstructure of Hardox 600 is martensite, which is what was found. The presence of longitudinal tempered martensite laths is visible in the microstructure. The rolling direction of the original sheet plate is visible with the presence of wide longitudinal martensite bands.

As mentioned the Hardox600 is a sheet plate which is made by rolling. The figure 5.2 shows noticeable longitudinal martensite bands(wide light lines in the microstructure). These bands could potentially indicate the direction in which the original sheet plate was rolled. It's worth noting that the crushing direction for the rings aligns with this as well. Given that it was not possible to examine the microstructure of the rings before the wear test, drawing any concrete conclusions regarding this aspect is challenging at this point.

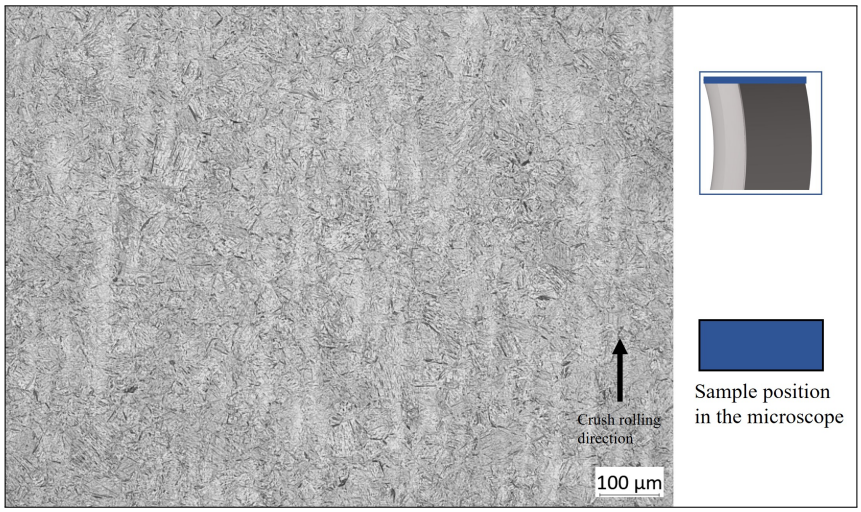

Figure 5.2: Martensite structure with presence of bands observed by optical microscope

The microstructure reveals a distinct contrast between the areas near the worn surface and the more distant regions, or middle parts, as shown in figure 5.3. The etching effect is more pronounced at the locations close to the surface. This noticeable contrast might come from various factors. For example, one possibility is that the etchant might have become trapped in the space between the mounting and the sample due to the unevenness of the worn surface, which caused prolonged contact of the etchant leading to more overetched-like microstructure. However, other hypothesis should also be considered:

- **Heat during crushing**: During the crushing process, the significant heat generated can alter the microstructure near the surface. Therefore, the observed inconsistencies in the microstructure and etching response might be attributable to variations in the heat process.

- **Plastic deformation**: The process of crushing abrasives could introduce internal stresses close to the rings' surface. This stress field could trigger plastic deformation, which in turn might lead to strain hardening of the surface areas. Consequently, this work-hardened regions could contribute to observable differences in the microstructure after etching.

In figure 5.4, a comparison of the microstructure from the surface and bottom on the cross-section of the samples is presented using SEM imaging. It's noticeable that the surface region has undergone significant grooving, a feature that will be further

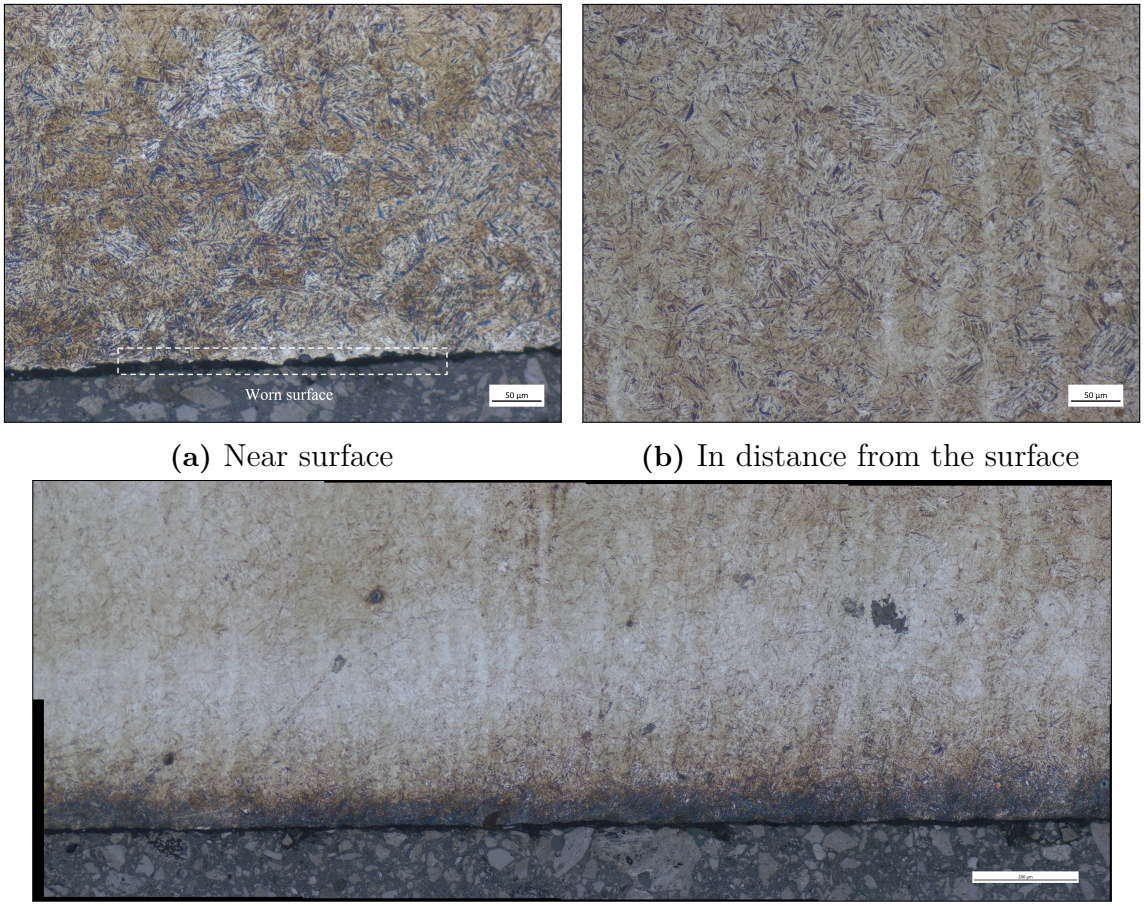

(a) Near surface

(b) In distance from the surface

(c) Overall view of the microstructure

Figure 5.3: Optical microstructure difference in the cross-section between surface regions and distant from the surface

explored in the surface analysis section. It becomes apparent that martensite bands near the surface have been deformed, aligned along the direction of the applied stress. However, this contrasts with the bottom regions of the ring, where the formation of martensite blocks does not appear to be altered. Based on these observations, we can infer that there might have been some degree of plastic deformation near the surface, possibly leading to a degree of work hardening. Further investigation, including a micro-hardness test detailed in the upcoming section, will provide additional insights to support or challenge this hypothesis.

5.2.1 Micro-hardness

As noted in the earlier section, it is plausible that a degree of plastic deformation may have occurred, especially in regions near the surface. To explore this hypothesis, a micro-hardness profile test was performed. Prior to delving into any results, it should be highlighted that Hardox 600 has undergone a quenching and tempering process, which would likely impact the hardness results. The sample that was used for this test is the cross-section sample (refer to figure 4.3). Three rows of indentations on the width of the sample, one in the right side,middle and left part of the sample, has

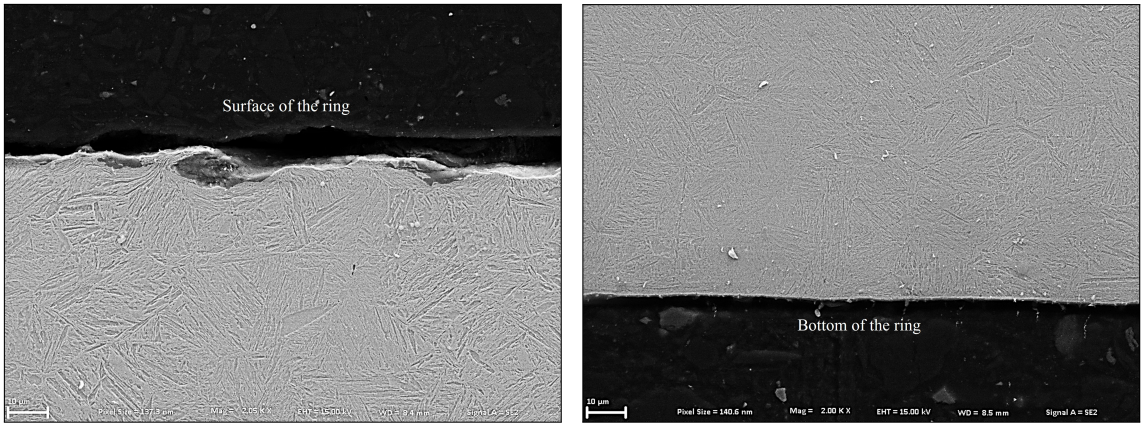

(a) Near surface of the ring **(b)** Near bottom of the ring

Figure 5.4: SEM comparison of surface and bottom region on cross-section

been applied. Detailed results of each row can be seen in appendixB The average of these has been considered as the overall values for the hardness profile. In figure 5.5, you can see the micro-hardness profile along the thickness of the Hardox 600:

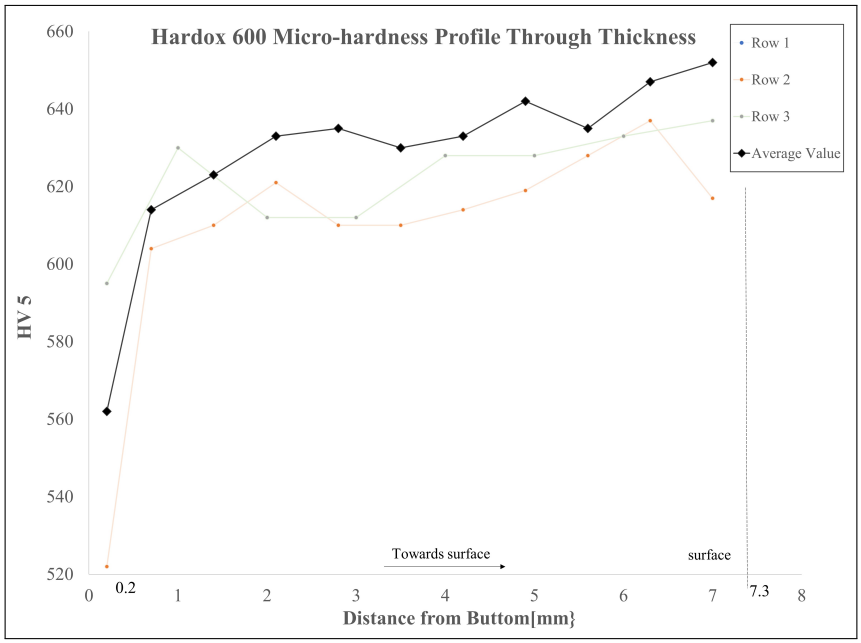

Figure 5.5: Micro-hardness profile through thickness of Hardox600

As can be seen, the hardness profile shows a steady increase from the bottom to the surface region. Considering the impact of heat treatments, the observed hardness increase, particularly close to the worn surface regions, corroborates the hypothesis of work hardening in these areas.
A notable observation is the significantly lower hardness in the initial indentations close to the sample's bottom edge. Even though they are 0.3mm away from the edge, this pronounced difference could be attributed to the edge effect in the micro-hardness test.

5.2.2 Stereo Microscope observation of the worn surface

As mentioned in the 4.1.3 the only way to monitor the wear during the test was the stereo microscope. In the figure 5.6.
After the third run, the ring surfaces were noticeably roughened, as illustrated by the transformation in topography. Some dark spots, which appear as holes in the rings, are visible in figure 5.6a. Upon closer examination using higher magnification, it was found that these dark spots are caused by significant variations in surface levels across different areas.

(a) 7.5x magnification

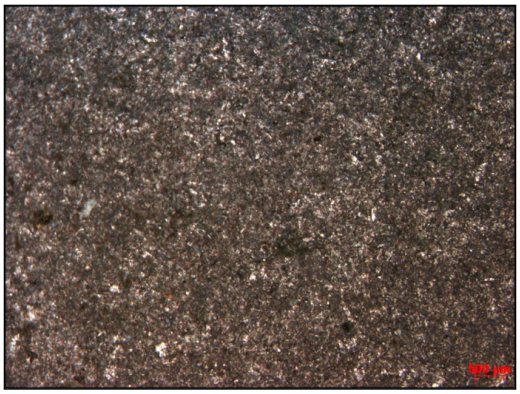

(b) 15x magnification

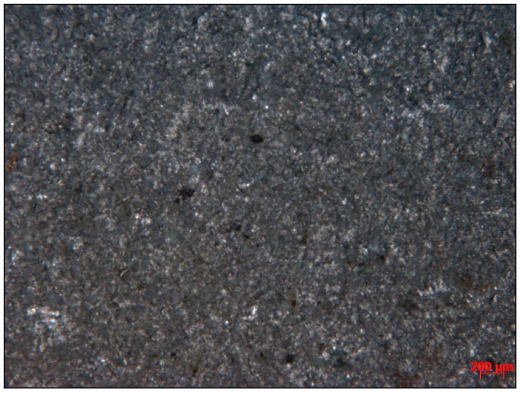

(c) 25x magnification

Figure 5.6: Stereo microscopy pictures of Hardox600 rings after third run

After six run some small changes in the surface can be seen, as shown in figure 5.10. But, these changes aren't very substantial. Looking at the pictures, it is not clear if the surface has gotten rougher or not. It seems like the surface is still not even, just like it was before(Run 3). The most noticeable alteration was the emergence of significant disparities in surface level, almost resembling material peeling off. This change was observed in various regions of the rings after the sixth run, a feature that wasn't apparent after the third run. (See figure 5.7c)

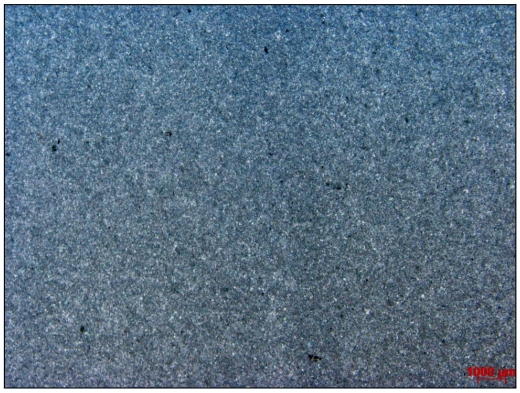

(a) 7.5x magnification

(b) 15x magnification

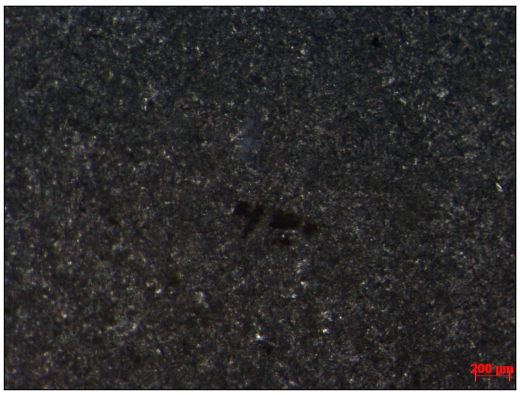

(c) 25x magnification

Figure 5.7: Stereo microscopy pictures of Hardox600 rings after sixth run

5.2.3 SEM and EDX analysis

To study the worn surface, sample a was used(refer to figure 4.3). The analysis consists of SEM, EDX, and BE to gain a comprehensive understanding of the wear occurring on the Hardox surface. A broad view of the surface can be found in figure 5.8, where the surface roughness is quite apparent. Given the challenges of distinguishing between Hardox material and abrasives, BE was used to clarify the features. The areas appearing darker in the image signify the embedded rocks, while the brighter areas show the worn surface of the Hardox600 material. As displayed, about half of the area (in the context of this image) is embedded with abrasive particles(rocks). The combination of the rings' relative movement and the contact pressure exerted between the rings and rocks during rock grinding could account for this embedding phenomenon. As will be discussed subsequently, these embedded rocks play a crucial role in understanding the wear mechanism and how the material is removed during the wear process.

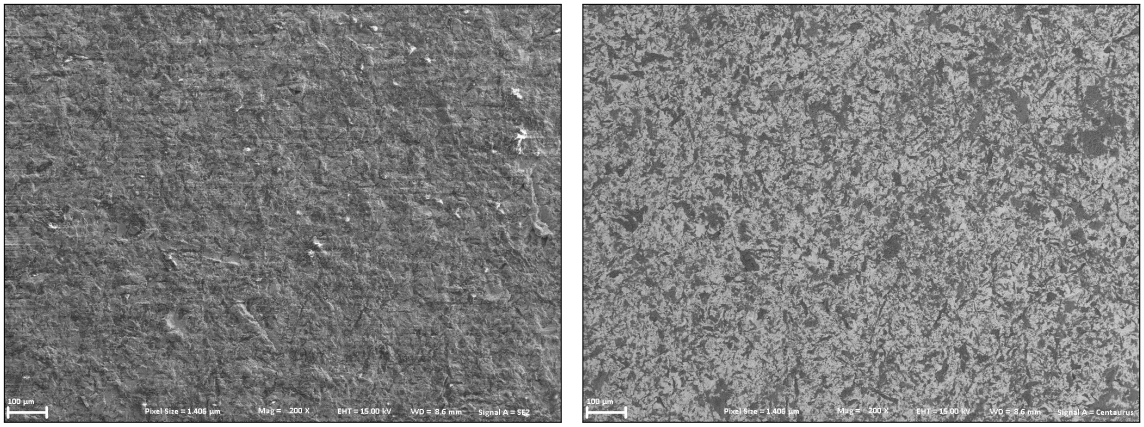

(a) SE image of surface **(b)** BE image of surface

Figure 5.8: SEM image of Hardox600 surface with presence of embedded rocks

To gain a clearer understanding of the surface's characteristics, EDX was performed for a chemical mapping of the surface. The comparison of the BE image and chemical map can be seen in Figure 5.9 These analyses complement each other as the embedded rocks, represented as dark regions in the BE image, also appear as Si elements in the chemical map.
Interestingly, varying shapes of these embedded rocks can be seen on the surface. Two distinct forms are present on the surface: one displays a flake-like shape, while the other exhibits a striation-like pattern.

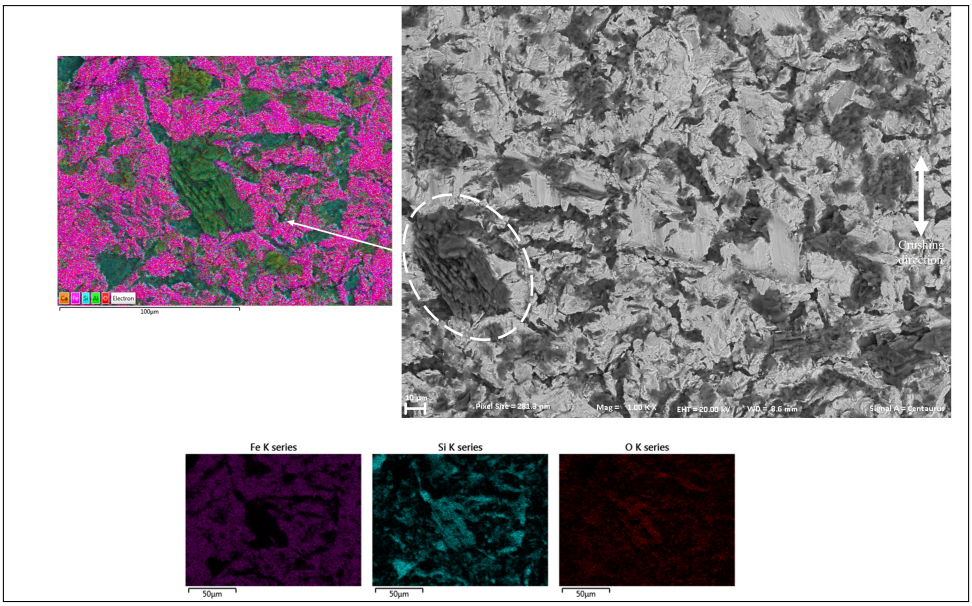

Figure 5.9: Chemical mapping of Hardox 600 surface: a)BE image b)Chemical map C)Element image

Apart from the embedded rocks, the SEM images offer insights into the Hardox material itself. It appears that the surface predominantly suffers from a cutting mechanism, as discussed previously. Evidence of material displacement, or 'ploughing,' can be seen in figure 5.10d with the direction of this ploughing mostly aligned

with the direction of rock crushing.

An understanding of the wear process can be drawn from the study of both the embedded rocks and the material displacement. It is hypothesized that following the initial contact and impression of the sharp abrasive into the material, rotation is induced. This causes a sliding across the surface, leading to observed ploughing. These ploughs often appear to be trapped between various embedded rock regions. (Refer to figure 5.10d)

Further examination suggests a hypothesis. It is suggested that once these embedded rock regions are formed, any subsequent ploughing continues until encountering these embedded rocks. These rocks, therefore, may act as a barrier, inhibiting the ploughs from further cutting into the surface.

An additional noticeable feature on the surface is the presence of material slivers dispersed across it. These slivers exhibit a flake-like appearance, almost suggesting a separation or detachment from the surrounding material. This particular characteristic can be attributed to the impact of the abrasives on the surface.

As described, the crushing mechanism involves a cyclic rotation of the rings, thus continuously crushing the rocks. The compression of the rock against the surface, which indents the sharp abrasives into it, is likely to induce a certain degree of deformation, as previously proposed. Each cycle of this repeated deformation, accompanied by the indentation of the abrasives, results in a tearing effect on the material. This is likely to contribute to the observed delamination and the formation of slivers.

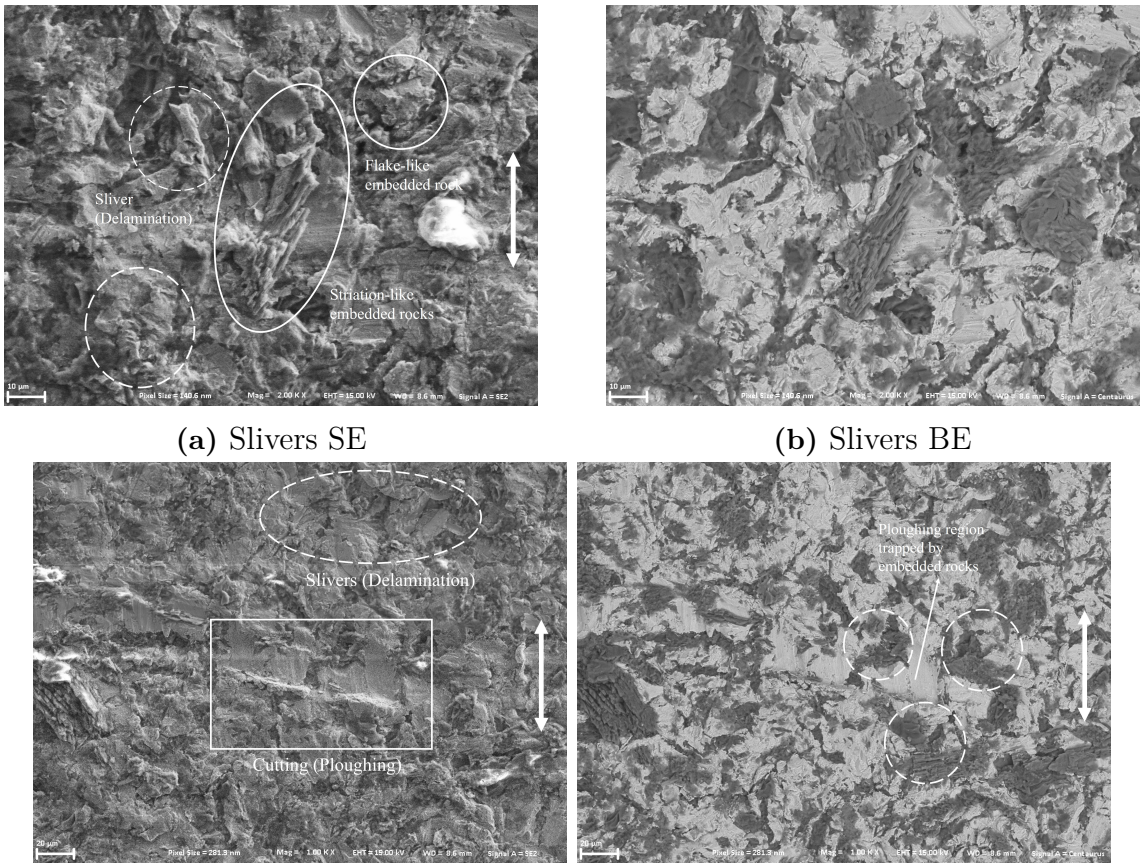

(a) Slivers SE **(b)** Slivers BE

(c) Ploughing SE **(d)** Ploughing BE

Figure 5.10: SEM material removal

5.3 Characterization of sintered X1 and X2

In this study, two different variants of WC with Co matrix are employed. The primary difference between them lies in the proportions of WC and Co - the sintered X1 material contains a lower proportion of WC and a higher proportion of Co compared to the sintered X2. As these materials were crafted specifically for this wear application rather than being commercially available products, there is limited information about the sintering process and its parameters.
First, a detailed examination of the materials' microstructure will be conducted. This will be followed by an analysis of the surface features, just as was carried out for the Hardox600 material.

5.3.1 Microstructure

After the completion of the wear test, cross-section samples were extracted from the Sintered X1 and X2 rings. These samples were subjected to a sequence of grinding, polishing, and etching. The microstructures of the sintered materials, X1 and X2, are depicted in Figure 5.11. Here, one can observe the dispersion of WC particles within the Co matrix. The WC particles are irregularly shaped, with various sizes.

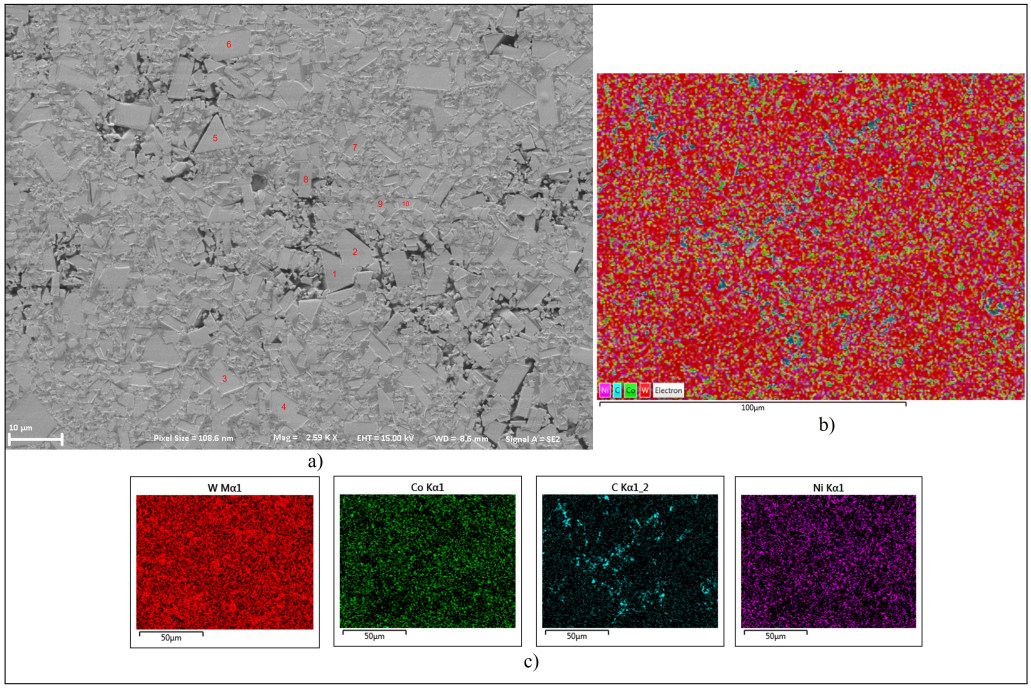

(a) Sintered X1

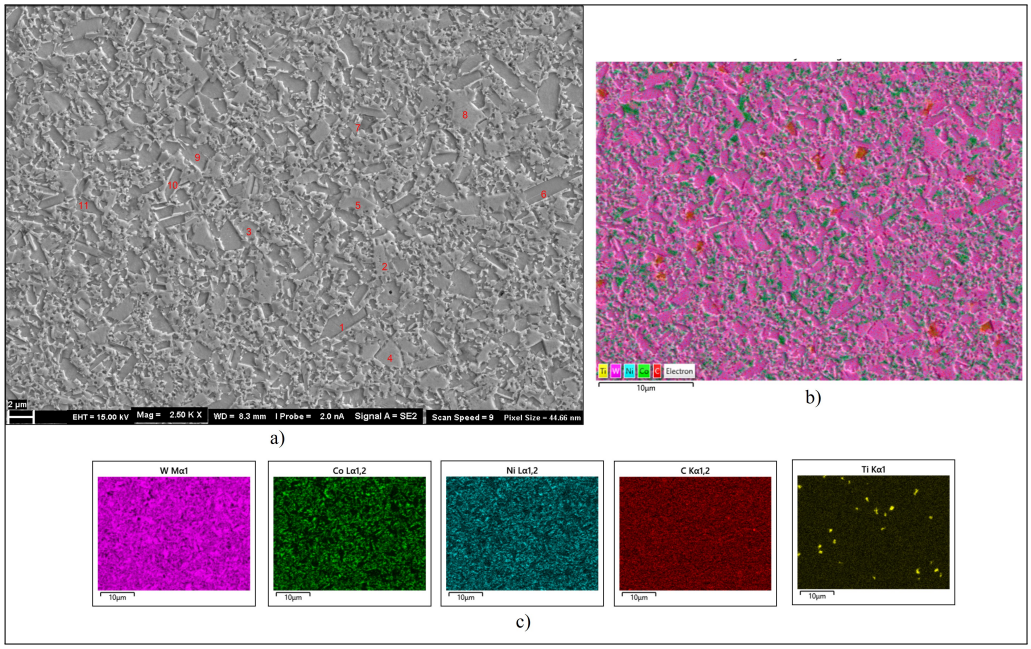

(b) Sintered X2

Figure 5.11: Microstructural analysis of sintered WC with Co matrix: a)SEM image b)Chemical mapping c)Elemental mapping of the cross-section sample

Upon comparing the microstructures of X1 and X2, it's evident that the WC particles in X1 are considerably larger than those in X2. In addition, the dispersion of WC particles in X2 is more uniform, demonstrating less size variation between the largest and smallest WC particles than X1.
To provide a more quantitative analysis, the ImageJ software was utilized to deter-

mine the sizes of the WC particles and calculate the respective 'Area' values. The data pertaining to the measured particles can be found in Table 5.1.

Table 5.1: Comparison of WC particle size between sintered X1 and X2

WC Place	WC X1 Area [µm^2]	WC X2 Area [µm^2]
1	27,296	4,362
2	32,182	2,557
3	21,711	1,689
4	28,612	2,915
5	25,669	4,531
6	40,589	4,312
7	9,866	1,596
8	15,735	6,541
9	5,704	4,1947
10	6,059	1,996
11	1,304	1,773

Corresponding to the measured WC particles from Figure 5.11 and Table 5.1, we can see that sintered X1 has WC particles from largest 40 µm^2 to smallest 1 µm^2. This is in contrast with the sintered X2 as the largest WC is 6.5 µm^2 and smallest 1 µm^2.

Figure 5.11 presents the EDX analysis results, offering insights into the chemical mapping and elemental breakdown of the observed surface. This analysis reveals the distribution and presence of various elements such as Tungsten, Cobalt, and Carbon, among others. The comparison of the overall elemental compositions for the sintered materials X1 and X2 is provided in Table 5.2.

Table 5.2: Elemental difference between sintered X1 and sintered X2

Elements	**Sintered X1 (Wt%)**	**Sintered X2 (Wt%)**
Tungsten (W)	68,2	77
Cobalt (Co)	8,7	10,6
Ni(Ni)	9,4	1,7
Titanium (Ti)	0,4	0,3

Given the superior wear performance of the sintered X2 material compared to the other materials tested, we can propose the following hypotheses about the wear resistance of sintered rings:

- **Tungsten Carbide Content**: Increasing the amount of tungsten in the material appears to enhance its wear resistance.
- **Size and Dispersion**: Utilizing smaller WC particles and achieving a homogeneous distribution of these particles within the matrix seem to boost the wear performance.

We should note that limitations inherent to the manufacturing process of these materials have not been factored into this comparison. Despite the two materials

having been produced by the same manufacturer, numerous manufacturing parameters could differ, such as the conditions under which sintering occurred, the type of powder and matrix employed, and more. Each of these factors could considerably influence the overall performance of the material.

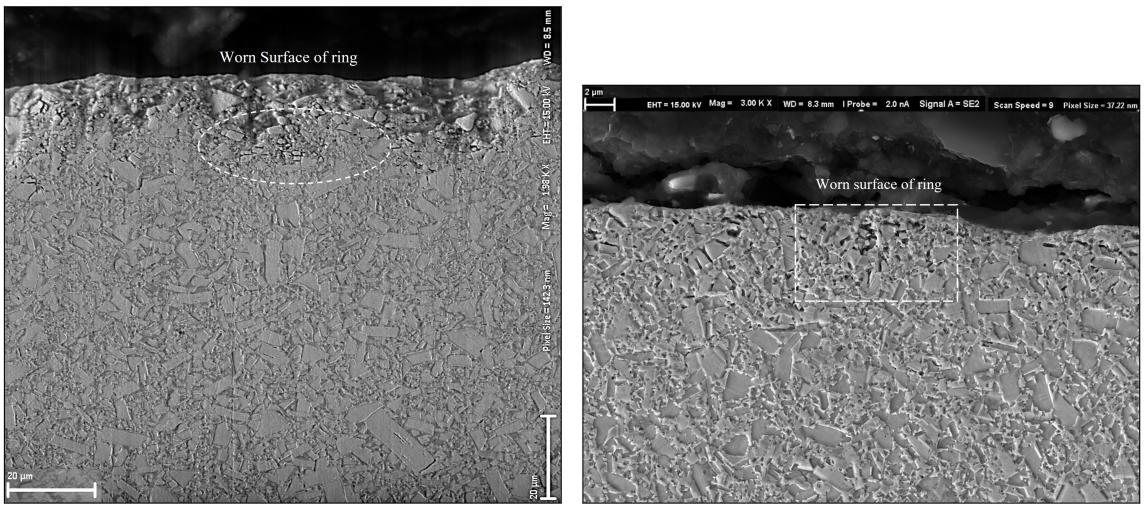

(a) SEM image for Sintered X1 **(b)** SEM image for Sintered X2

Figure 5.12: Comparison of the microstructure near-surface region on cross-section

Figure 5.12 shows the microstructure from the surface regions of the sintered X1 and X2 rings on the cross-section.
On first inspection, we see noticeable differences in the extent of wear between the sintered rings. The surface of the sintered X1 ring is visibly rougher than that of the X2 ring. This observation is supported by the unevenness across the top layer of the X1 cross-section, indicative of its worn surface. Upon closer examination, we notice that wear has caused extensive damage to the WC particles in the X1 sample, resulting in significant material removal from the surface. This level of wear is not as prominent in the sintered X2 sample, which aligns with our experimental wear results.
A more detailed look at the SEM images reveals additional differences. For the sintered X1, we see micro-cracks and fractures within the WC particles near the surface. In contrast, the sintered X2 ring shows a different worn surface: WC particles near the surface have merely detached from the matrix binder due to the stresses incurred during crushing, with far fewer observed fractures within the WC particles.

5.3.2 Micro-hardness

Similar to the procedure employed for the Hardox600, we also evaluated the hardness through the thickness of the sintered rings. The cross-section samples were utilized for this examination. We performed hardness tests in three rows, each indentation separated by a distance of 0.7mm along the thickness. Detailed hardness values for

each of these rows can be found in Appendix B.

Figure 5.13 illustrates a comparison of the hardness profile through the thickness of both sintered X1 and X2 rings. It can be observed that there are variations in the hardness throughout the thickness. These fluctuations can be attributed to the inherent non-uniformity of the sintered material, with possible variations in the distribution of matrix and hard phases. This suggests that regions of lower hardness might have a higher binder content and a lower presence of hard phases. Furthermore, the variability in the shape and size of the WC particles throughout the sample might also contribute to these fluctuations.

Interestingly, both sintered rings show a similar trend of hardness increasing from the bottom regions towards the surface. This trend mirrors the one observed for the Hardox600.

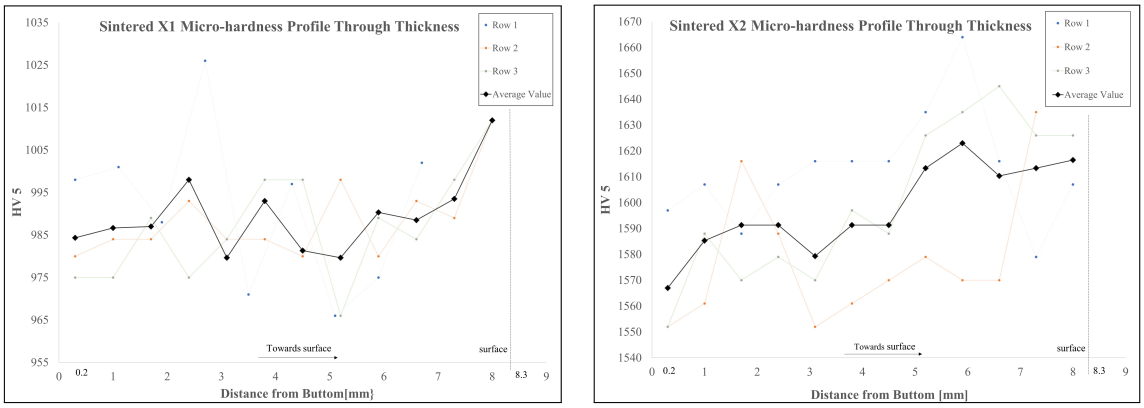

(a) Sintered X1 **(b)** Sintered X2

Figure 5.13: Hardness profile of sintered rings through thickness

In addition to the hardness testing, we performed indentation experiments near the surface areas of the sintered rings to observe their responses. We used the same HV5 method for these indentations.

Upon indentation, as shown in Figure 5.14 only the upper surface areas of the sintered X2 material exhibit cracking. In contrast, the sintered X1 material does not display this cracking behavior.
This cracking in the top surface areas of sintered X2 could be attributed to the loading during hardness measurement. X2, with its higher WC content, exhibits increased brittleness and decreased toughness. As a result, it is more susceptible to crack formation. When an indentation load is applied, these stresses trigger the formation of cracks and lead to material breakage. The absence of such behavior in sintered X1 might be attributed to its higher matrix content, which could make the material more prone to plastic deformation in its softer regions. As a result, the internal stresses would tend to deform these softer areas, rather than creating high-stress zones in the detached WC.
Regardless of the cause of this crack, its exclusive appearance in the sintered X2 is

noteworthy. Similar to what was discussed in section 2.4.2.3, the brittle characteristics of the sintered X2 are evident from the way the crack initiates and extends to the surface.

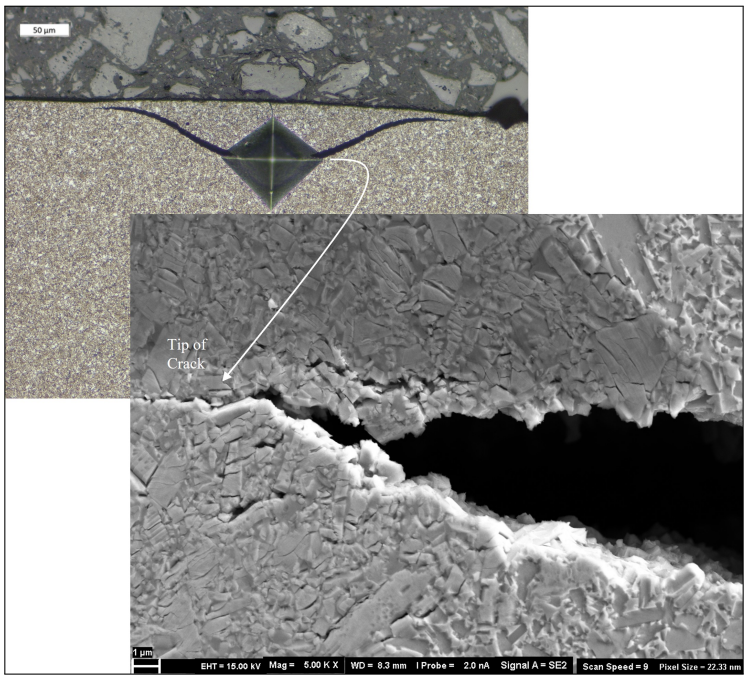

Figure 5.14: SEM image of crack appeared after indentation on sintered X2

5.3.3 SEM and EDX analysis

Similar to the analysis performed on the Hardox600 ring, SEM and EDX analysis were conducted to investigate the changes in surface topography. Comparison between the two sintered rings, X1 and X2, helped to gain a better understanding of the surface differences resulting from wear.

Figure 5.15 provides SEM images of the worn surfaces of X1 and X2. From the figure, it is evident that the two materials exhibit varying degrees of wear. This disparity is most noticeable in the black regions scattered across the surface. With comparing with the EDX analysis, these black regions visible in both X1 and X2, are probably compressed rocks that got embedded during the crushing.
The worn surface of the material is subjected to EDX analysis in Figure 5.16. The dark areas in the SEM image are identified as areas where oxygen is present. This oxygen presence could be attributed to two possible sources: embedded rock contaminants or oxidation of cobalt when exposed to air. However, cobalt oxidation is not easily triggered at ambient temperatures; it usually occurs at higher temperatures. Hence, the presence of oxygen and silicon can be more reasonably attributed to embedded rock contaminants.

The elemental analysis of these areas reveals a deficiency (or very low levels) of Tungsten, Carbon, and Cobalt. This implies that the material from these areas has

likely been stripped away from the surface. There are two potential mechanisms for this behavior:

- The first mechanism involves the effects of local stresses experienced during the crushing process. The stress field near the surface region could result in detachment between WC particles and the Cobalt matrix, leading to the removal of material from the surface. This effect is similar to what was observed in the cross-section figure (refer to Figure 5.12). The resulting cavities on the surface could be seen as evidence of this phenomenon.
- The second mechanism suggests that Cobalt, being the softer component of the material, would experience wear before the harder WC. This wear could eventually lead to the detachment of WC particles from their surrounding matrix, leading to cavities.

The images provided in Figures 5.16a and 5.16b demonstrate that these small cavities can merge over time. These cavities tend to act as stress concentration sites, and as the materials endure further stress from impacts and friction during the crushing process, these cavities expand. Ultimately, they merge with adjacent cavities, resulting in larger cavities.

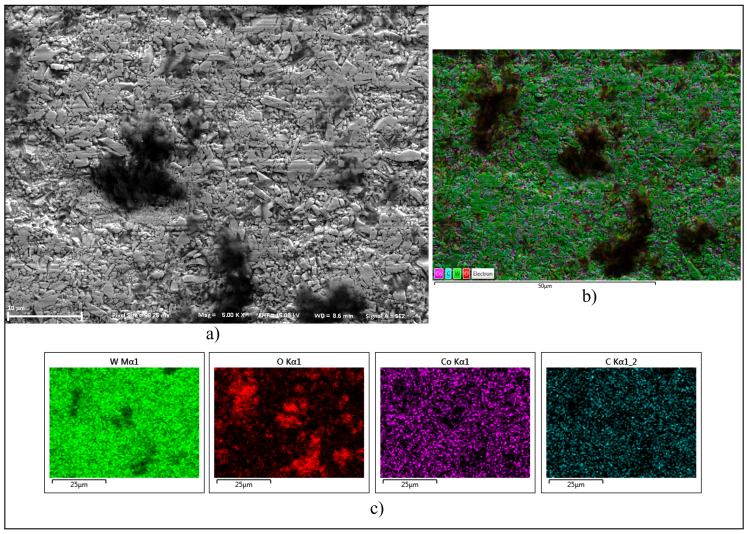

Figure 5.15: Chemical mapping of Sintered X2 surface: a)SEM image b)Chemical map C)Element map

By observing the surface topography, we can see clear differences in the extent of wear when comparing the surface roughness of X1 and X2. Apart from the previously discussed cavities, X2 presents a predominantly smooth surface, indicating it has not undergone extensive wear. This surface texture is consistent with the experimental wear result (refer to figure 5.1). Upon examining at higher magnifications, it is apparent that the surface has primarily experienced microcracks and cracks within the WC particles, leading to fractures and particle detachment from the surface (refer to figures 5.16d and 5.16f).

On the other hand, X1's surface is quite rugged with many notable 'peaks and

valleys'. As shown in figure 5.16c, a form of "cutting" behavior, akin to what we observed for the Hardox600, can be seen for sintered X1 as well. Despite the stark difference in hardness due to their different compositions, the presence of soft Co binder could drive wear in a particular direction, creating a surface feature reminiscent of a cutting mechanism but distinct from the ploughing observed on the Hardox600 surface.

A possible explanation could be that the higher content of Cobalt and Nickel in sintered X1 leads to the preferential removal of the Cobalt matrix surrounding the hard phase (WC). This exposes WC particles more directly to rock abrasives, facilitating directional wear that might be mistaken for "cutting".

The increased content of Cobalt and Nickel in the binder phase could also affect the wear process in other ways. When comparing figures 5.16a and 5.16b, it is evident that sintered X1 has more numerous and larger cavities compared to X2. As we've noted, these cavities can expand and coalesce. More soft elements like Cobalt and Nickel could facilitate this merging process, as they might provide more initial cavity sites. Additionally, the "cutting" mechanism we discussed for X1 could enhance the growth of individual cavities, making it easier compared to sintered X2.

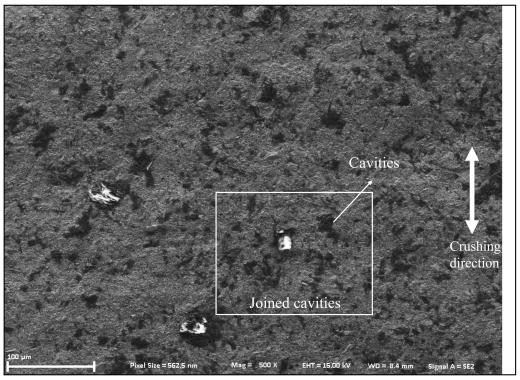

(a) Sintered X1 at 500x magnification

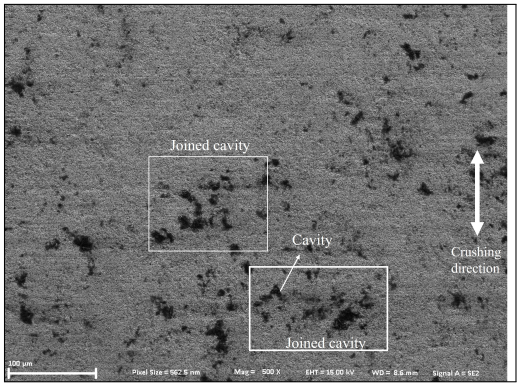

(b) Sintered X2 at 500x magnification

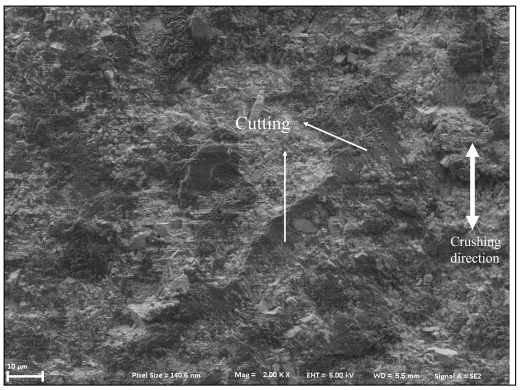

(c) Sintered X1 at 2k magnification

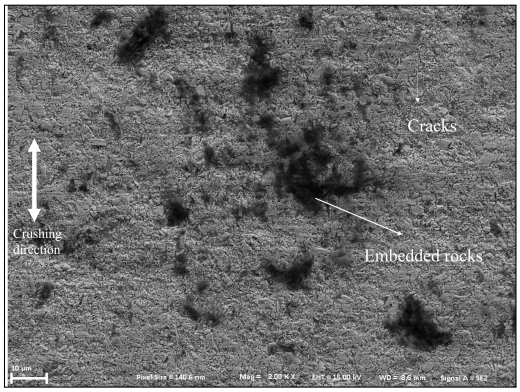

(d) Sintered X2 at 2k magnification

(e) Sintered X1 at 5k magnification

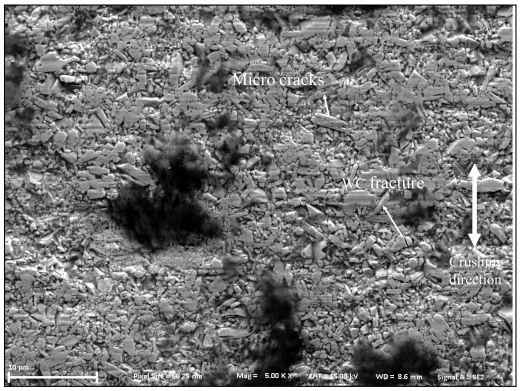

(f) Sintered X2 at 5k magnification

Figure 5.16: SEM comparison of sintered surfaces at different magnifications

6
Discussion

The wear behavior exhibited by the tested materials varied significantly, as evidenced by the unique changes in surface topography and cross-section appearance after wear. These findings underscore the unpredictability of wear, even within the same application.

Given the nature of the crushing principle and similarities with wear studies on the CRS machine, discussed in the theory section, it's fair to conclude that the machine endures high-stress three-body abrasive wear. Recognizing this wear type is essential as it highlights the importance of the characteristics of the abrasives as part of the entire tribosystem, alongside the ring materials. Therefore, to improve wear resistance, the entire system should be considered, not just the ring materials.

Each material responded uniquely to this abrasive wear. To provide a comprehensive understanding of the wear mechanisms, we've proposed several hypotheses for each material that capture the overall process and potential occurrences during wear. These hypotheses will be divided among the tested materials.

6.1 Hardox600

As determined from our results, the primary wear mechanisms causing material loss were cutting, manifested as surface ploughing, and a form of strain fatigue due to cyclic plastic deformation, visible as surface slivers.

Drawing on the results and two analogous studies about three-body impact abrasive wear [39, 40], we can propose the following hypothesis to explain the wear behavior of Hardox 600, as shown schematically in Figure 6.1:

- Initially, the abrasive rocks are compacted into the gap between the rotating rings, where sharp rock particles create indentations on the surface, triggering surrounding plastic deformation.
- Following the indentation, the rotation of the rings causes the indented rocks to slide across the surface, which leads to a phenomenon known as ploughing.
- The sliding motion of the abrasive particles pushes material ahead of it, forming surface protrusions, known as asperities.
- These asperities encounter cyclic contact with the abrasives, which leads to

their gradual dislodgment into slivers.

- As indentation at a specific site increases, the indented rocks compress together to form an embedded rock region. These embedded rocks inhibit further surface cutting. This is evidenced by the trapped ploughing regions surrounded by embedded rocks.

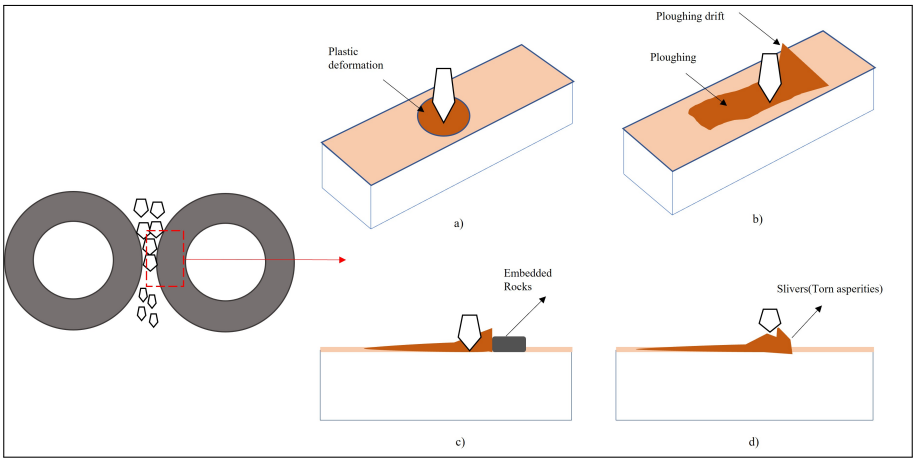

Figure 6.1: Schematic of wear mechanisms on Hardox600: a)Indentation of rocks on surface b)slide of rocks c)hindering of ploughing d)tearing of asperities(formation of slivers)

6.2 Sintered WC/Co

The results showed that the sintered rings exhibited remarkably different wear behavior compared to Hardox600. The damage to the surface was due to several distinct mechanisms: Matrix removal, WC fracture, and the detachment of WC from the matrix. These processes eventually resulted in either the matrix, WC, or both being peeled off from the surface during wear.

Similar to Hardox600, based on the observed mechanisms on the surface and microstructure, we can propose a general hypothesis about the wear process on the sintered surfaces, as shown schematically in Figure 6.2:

- When rocks are compressed against the surface, two different scenarios might occur:
  1. The rocks could indent the surface and dislodge the matrix binder, which would detach WC particles from their surrounding binder. These loosened WC particles could then be peeled off or fractured upon contact with other abrasives during the crushing process. This scenario is consistent with the behavior observed in Sintered X1.
  2. Alternatively, the rock might not penetrate the surface but could induce residual stresses beneath the surface. These stresses could cause WC to detach from its surrounding matrix, leading to the peeling off of WC particles and their boundaries from the surface. This scenario corresponds to the behavior observed in Sintered X2.

- These grain peel-offs on the surface, due to the aforementioned mechanisms, appear as cavities on the surface. These cavities can expand and merge with nearby cavities, forming larger cavitation sites. The results indicated that the growth and merging of cavities were more pronounced in Sintered X1 compared to X2. This difference is likely due to the softer nature of X1, which contains more binder content compared to X2.

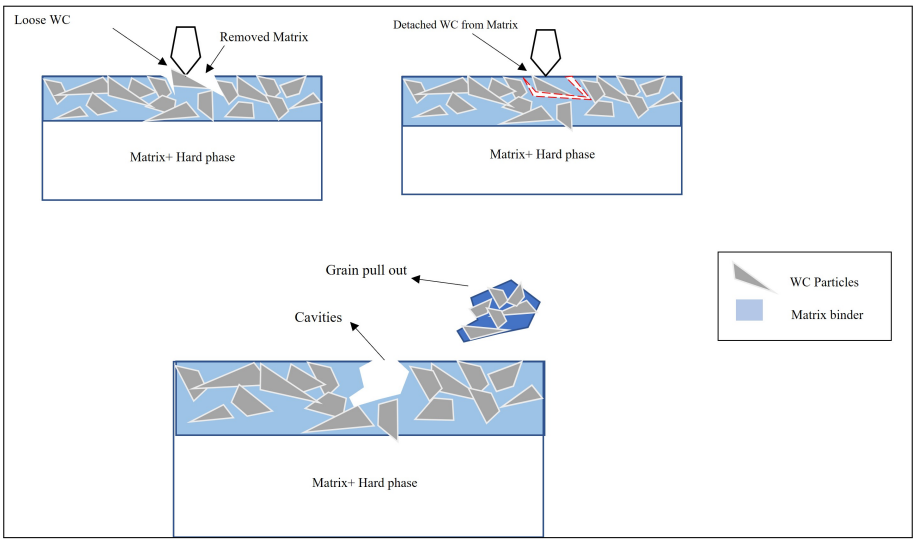

Figure 6.2: Schematic of wear mechanisms on sintered rings

The discrepancy in wear behavior exhibited by the sintered rings is primarily due to their differences in hardness and the distinct compositions of their matrix and hard phase constituents. This is evident from the results as well as from previous research exploring the abrasive characteristics of WC in matrix rings. These studies confirm that with increasing WC grain size, the hardness and compressive strength of the material decrease [41].

Transverse rupture strength is a crucial characteristic of hard particles like WC, reflecting its durability against fracture or bending. It's established that WC particles display peak transverse rupture strength at around $3\mu m$ in size. For sintered carbides with smaller WC particles, wear primarily manifests in the cobalt region. In contrast, larger WC particles experience wear and fracture themselves. Moreover, a wider distribution of WC particle sizes within the matrix has been shown to yield greater rupture strength [41].

A study on the properties of sintered carbides asserts that to achieve optimum abrasive wear resistance, sintered WC with a Co matrix should contain 3-13% Cobalt and have a grain size of 2-6μm, particularly for mining applications [42].
The 'mean free path' in the matrix is a key characteristic of sintered carbides, denoting the thickness of cobalt layers. This measurement depends on both the cobalt content and the WC particle size, and it is inversely proportional to hardness. Analysis shows that a reduction in cobalt content and WC particle size yields a shorter mean free path, implying an increase in hardness [41].

These findings highlight the significant role of hardness plays in this specific high-stress, three-body abrasive wear. While hardness on its own cannot be the principal property predicting wear behavior, it's clear in this type of wear that a decrease in hardness can result in severe wear damage.

7
Conclusion

The comprehensive conclusion drawn from analyzing the entire wear tribosystem is presented here.

- The wear behavior varies significantly among the tested materials. These variations are evident in the changes observed in both the surface topography and the microstructure after wear.
- The materials can be ranked from the most resistant to the least as follows: Sintered X2, Sintered X1, and Hardox600.
- Evaluating the crucial parameters of the tribosystem, it's discerned that the wear mode of the CRS crushing machine is characterized by high stress three-body abrasive wear.
- Based on the materials tested, it's clear that hardness is the predominant factor in determining wear for this specific scenario. Materials that undergo plastic deformation experience more intense wear, as observed with Hardox600. Conversely, when materials exhibit high strength/hardness, wear tends to be more manageable, as seen with Sintered WC/Co.

Hardox600:

- The primary mechanisms driving material removal are cutting and repeated plastic deformations that occur on the surface asperities visible on the surface as the "ploughings", and "slivers".

Sintered WC/Co:

- Various mechanisms contribute to material removal, such as matrix extraction, the development of microcracks, fracturing of WC particles, WC particles becoming detached from the matrix, and grain pull-outs. Over time, cavities may coalesce.
- Materials with a greater WC content, characterized by a more diverse size distribution (both smaller and larger), exhibit enhanced wear resistance and hardness. This composition also ensures optimal performance during the fracture of WC particles.

Abrasive characteristics:

- The abrasive characteristics play a pivotal role in wear behavior. The distinction between plastic or brittle responses in a material hinges on its comparative hardness to that of the abrasive. If the abrasive's hardness exceeds the material's hardness (by at least 1.2 times), the material will predominantly display a plastic response, regardless of its innate hardness.

Future Works

The primary aim of this thesis was to better comprehend the wear behavior during compressive crushing. Given the innovative nature of the crushing mechanism, there's a lack of studies aimed at enhancing wear properties.
The wear tests executed in this study were limited to a specific test method configuration. It's crucial to note that wear is an intricate phenomenon largely influenced by the specific parameters of its associated systems. By varying certain machine parameters and analyzing wear in the same systematic manner as in this project, we can attain a more complete understanding.

Factors that could significantly influence wear and are worth considering for future research include:

- **Rock Feed Size:** Altering the feed ratio during consecutive runs may lead to distinct wear patterns.
- **Initial Feed Mass:** A greater mass would lengthen the crushing time in each run, providing insights more reflective of real-world applications.
- **Lubrication:** All tests were performed in dry conditions. Assessing wear in wet conditions or with various lubricants can provide insights into potential changes in wear rate and mechanisms.
- **Volumetric Mass Between Gaps:** This can be varied to observe its effect on wear.

Given the current machine's limitations, especially the prolonged testing duration, one viable approach is to compare the wear results of the existing CRS machine with standard three-body abrasive wear tests, such as ASTM B611. If the outcomes from these standard tests align closely with the CRS findings, they could greatly facilitate scaling up investigations across different tribosystem parameters.

Materials Selection:
While the sintered WC/Co X2 showcased commendable wear performance in our tests, its manufacturing challenges could cause it commercially less viable. Further research might explore alternative techniques, such as Laser cladding or High-Velocity oxygen fuel (HVOF), which might be more suitable for commercial applications.

Bibliography

[1] J. Jeswiet and A. Szekeres, "Energy Consumption in Mining Comminution," in *Procedia CIRP*, vol. 48. Elsevier B.V., 2016, pp. 140–145.

[2] S. K. Kawatra, *Advances in comminution*. Society for Mining, Metallurgy, and Exploration, 2006.

[3] Marc Allen, "MINING ENERGY CONSUMPTION 2021 A high-level study into mining energy use for the key mineral commodities of the future," Tech. Rep.

[4] B. A. Wills and J. A. Finch, "Crushers," *Wills' Mineral Processing Technology*, pp. 123–146, 1 2016. [Online]. Available: https://linkinghub.elsevier.com/retrieve/pii/B9780080970530000066

[5] H. Lieberwirth, P. Hillmann, and M. Hesse, "Dynamics in double roll crushers," *Minerals Engineering*, vol. 103-104, pp. 60–66, 4 2017.

[6] L. G. Austin, D. R. Van Orden, and J. W. Pi˜rez, "A PRELIMINARY ANALYSIS OF SMOOTH ROLL CRUSHERS," Tech. Rep., 1980.

[7] Y. Sesemann, C. Broeckmann, and A. Höfter, "A new laboratory test for the estimation of wear in high pressure grinding rolls," *Wear*, vol. 302, no. 1-2, pp. 1088–1097, 4 2013.

[8] P. Hillmann, M. Hesse, and H. Lieberwirth, "New horizons for double-roll crushers," *ESCC, Proceedings*, p. 233 – 239, 2015. [Online]. Available: https://www.scopus.com/inward/record.uri?eid=2-s2.0-85010795201&partnerID=40&md5=aa2430dc84a8d699e1ed4262295d776f

[9] J. Almen, *Mechanical Wear (ed J.T. Burwell)*.

[10] D.S., "Glossary of terms and definitions in the field of friction, wear and lubrication (tribology)," *Wear*, vol. 15, no. 6, 1970.

[11] U. Search and R. Activities, "Standard Terminology Relating to Wear and Erosion," *Current*, vol. 94, no. Reapproved, 1999.

[12] I. Hutchings, "The Challenge of Wear," in *Wear - Materials, Mechanisms and Practice*. Chichester, England: John Wiley & Sons Ltd, 9 2014, pp. 1–7.

[13] J. T. Burwell, "Survey of possible wear mechanisms," *Wear*, vol. 1, no. 2, 1957.

[14] Koji Kato and Koshi Adachi, "Chapter 7: Wear Mechanisms, Modern Tribology Handbook, Two Volume Set," Tech. Rep.

[15] K. H. Zum Gahr, "Chapter 4 Classification of Wear Processes," in *Microstructure and Wear of Materials*, ser. Tribology Series, K.-H. Z. Gahr, Ed. Elsevier, 1987, vol. 10, pp. 80–131. [Online]. Available: https://www.sciencedirect.com/science/article/pii/S0167892208707223

[16] H. . Czichos, K.-H. . Habig, and E. Santner, "Tribologie-Handbuch Reibung und Verschleiß ; mit 115 Tabellen." [Online]. Available: https://www.worldcat.org/title/76560305

[17] Koji Kato and Koshi Adachi, "Chapter 7: Wear Mechanisms, Modern Tribology Handbook, Two Volume Set," Tech. Rep.

[18] I. Hutchings and P. Shipway, "Wear by hard particles," *Tribology*, pp. 165–236, 1 2017.

[19] J. A. Hawk and R. D. Wilson, "Tribology of earthmoving, mining, and minerals processing," in *Modern Tribology Handbook: Volume One: Principles of Tribology*, 2000.

[20] M. Peterson and W. Winer, "Wear in ore processing machinery," in *Wear Control Handbook*. New York: ASME, 1980, pp. 1009–1051.

[21] P. Mutton, *Abrasion Resistant Materials for the Australian Minerals Industry*. Melbourne: Australian Minerals Industries Research Association Limited, 1988, vol. 1.

[22] G. W. Stachowiak and A. W. Batchelor, "11 - Abrasive, Erosive and Cavitation Wear," in *Engineering Tribology (Third Edition)*, third edition ed., G. W. Stachowiak and A. W. Batchelor, Eds. Burlington: Butterworth-Heinemann, 2006, pp. 501–551. [Online]. Available: https://www.sciencedirect.com/science/article/pii/B9780750678360500122

[23] G. Straffelini, "Surfaces in contact," *Springer Tracts in Mechanical Engineering*, vol. 11, pp. 1–20, 2015.

[24] M. V. Swain and B. R. Lawn, "Indentation fracture in brittle rocks and glasses," *International Journal of Rock Mechanics and Mining Sciences and*, vol. 13, no. 11, 1976.

[25] B. R. Lawn and E. R. Fuller, "Equilibrium penny-like cracks in indentation fracture," *Journal of Materials Science*, vol. 10, no. 12, pp. 2016–2024, 12 1975. [Online]. Available: https://link.springer.com/article/10.1007/BF00557479

[26] I. Kramer and L. Demer, "The effect of surface removal on the plastic behavior of aluminum single crystals," *TRANSACTIONS OF THE METALLURGICAL SOCIETY OF AIME*, vol. 221, no. 4, pp. 760–786, 1961.

[27] A. Misra and I. Finnie, "On the size effect in abrasive and erosive wear," *Wear*, vol. 65, no. 3, 1981.

[28] J. T. Fourie, "The flow stress gradient between the surface and centre of deformed copper single crystals," *https://doi.org/10.1080/14786436808223026*, vol. 17, no. 148, pp. 735–756, 2006. [Online]. Available: https://www.tandfonline.com/doi/abs/10.1080/14786436808223026

[29] M. Yuan, S. Karamchedu, Y. Fan, L. Liu, L. Nyborg, and Y. Cao, "A case study for a worn tool steel in the hot stamping process," *Journal of Materials Research and Technology*, vol. 22, pp. 1065–1075, 1 2023.

[30] SSAB, "Hardox 600 Data Sheet," SSAB, Tech. Rep.

[31] H. Bhadeshia and R. Honeycombe, "Strengthening of Iron and Its Alloys," *Steels: Microstructure and Properties*, pp. 23–57, 1 2017.

[32] K. Ligier, M. Zemlik, M. Lemecha, Konat, and J. Napiórkowski, "Analysis of Wear Properties of Hardox Steels in Different Soil Conditions," *Materials*, vol. 15, no. 21, 2022.

[33] G. Straffelini, "Materials for tribology," *Springer Tracts in Mechanical Engineering*, vol. 11, pp. 159–199, 1 2015.

[34] G. S. Upadhyaya, *CEMENTED TUNGSTEN CARBIDES. Production, Properties and Testing.*, 1998, vol. 5, no. 30 V.

[35] ——, "Production of Metal and Carbide Powders," *Cemented Tungsten Carbides*, pp. 55–88, 1 1998.

[36] ——, "Consolidation of Cemented Carbides," *Cemented Tungsten Carbides*, pp. 89–137, 1 1998.

[37] "Tables of Chemicals and Etchants," in *Metallography and Microstructures*. ASM International, 12 2018, pp. 1094–1114.

[38] M. Göransson, U. Bergström, and H. Shomali, *Beskrivning till bergkvalitetskartan del av Mölndals kommun*.

[39] Z. Pei, R. Song, Q. Ba, and Y. Feng, "Dimensionality wear analysis: Three-body impact abrasive wear behavior of a martensitic steel in comparison with Mn13Cr2," *Wear*, vol. 414-415, pp. 341–351, 11 2018.

[40] E. S. Zanoria, "Application of the ring-on-ring test for abrasive wear modeling of rolling undercarriage components in track-type machines," *Wear*, vol. 257, no. 1-2, pp. 205–214, 7 2004.

[41] H. E. Exner and J. Gurland, "A REVIEW OF PARAMETERS INFLUENCING SOME MECHANICAL PROPERTIES OF TUNGSTEN CARBIDE–COBALT ALLOYS," *http://dx.doi.org/10.1179/pom.1970.13.25.002*, vol. 13, no. 25, pp. 13–31, 2014. [Online]. Available: https://www.tandfonline.com/doi/abs/10.1179/pom.1970.13.25.002

[42] M. Antonov, R. Veinthal, D. L. Yung, D. Katušin, and I. Hussainova, "Mapping of impact-abrasive wear performance of WC–Co cemented carbides," *Wear*, vol. 332-333, pp. 971–978, 5 2015.

A

Appendix A

Here you can find detailed parameters of the experimental wear test data for each test.

Hardox600:

Test ID	Test	Gap [mm]	Rollers	Ore	Ore amount start [kg]	Ore amount end [kg]	Belt frequency [Hz]
A1	Hardox Compression 0.8	0,8	Hardox 600	Quarry Rock	59,9	59,4	60
A2	Hardox Compression 0.8	0,64	Hardox 600	Quarry Rock	59,4	59,2	60
A3	Hardox Compression 0.8	0,512	Hardox 600	Quarry Rock	59,8	58,8	47
A4	Hardox Compression 0.8	0,4096	Hardox 600	Quarry Rock	59,5	59,2	60
A5	Hardox Compression 0.8	0,32768	Hardox 600	Quarry Rock	58,4	57,8	43
A6	Hardox Compression 0.8	0,262144	Hardox 600	Quarry Rock	57,8	56,9	28

Sintered X1:

Test ID	Test	Gap [mm]	Rollers	Ore	Ore amount start [kg]	Ore amount end [kg]	Belt frequency [Hz]
B1	Sintered X1 Compression 0.8	0,8	Sintered X1	Quarry Rock	60,7	60,2	48
B2	Sintered X1 Compression 0.8	0,64	Sintered X1	Quarry Rock	60,2	59,8	53
B3	Sintered X1 Compression 0.8	0,512	Sintered X1	Quarry Rock	59,8	59,4	47
B4	Sintered X1 Compression 0.8	0,4096	Sintered X1	Quarry Rock	59,4	59,0	57
B5	Sintered X1 Compression 0.8	0,32768	Sintered X1	Quarry Rock	59,0	58,3	34,5
B6	Sintered X1 Compression 0.8	0,262144	Sintered X1	Quarry Rock	58,3	57,5	27,5

Sintered X2:

Test ID	Test	Gap [mm]	Rollers	Ore	Ore amount start [kg]	Ore amount end [kg]	Belt frequency [Hz]
C1	Sintered X2 Compression 0.8	0,8	Sintered X2	Quarry Rock	62,7	62,3	52
C2	Sintered X2 Compression 0.8	0,64	Sintered X2	Quarry Rock	62,3	62,0	57
C3	Sintered X2 Compression 0.8	0,512	Sintered X2	Quarry Rock	62,0	61,6	39
C4	Sintered X2 Compression 0.8	0,4096	Sintered X2	Quarry Rock	61,6	61,1	60
C5	Sintered X2 Compression 0.8	0,32768	Sintered X2	Quarry Rock	61,1	60,4	48
C6	Sintered X2 Compression 0.8	0,262144	Sintered X2	Quarry Rock	60,4	59,5	36

B

Appendix B

Here are the specific values from the micro-hardness tests conducted on the materials under examination.

Hardox600:

Row 1:

Indentation	Xdistance[mm]	Method	Hardness[HV5]
1	0	HV 5	562
2	0.7	HV 5	614
3	1.4	HV 5	623
4	2.1	HV 5	633
5	2.8	HV 5	635
6	3.5	HV 5	630
7	4.2	HV 5	633
8	4.9	HV 5	642
9	5.6	HV 5	635
10	6.3	HV 5	647
11	7	HV 5	652

Row 2:

Indentation	Xdistance[mm]	Method	Hardness[HV5]
1	0	HV 5	522
2	0,7	HV 5	604
3	1,4	HV 5	610
4	2,1	HV 5	621
5	2,8	HV 5	610
6	3,5	HV 5	610
7	4,2	HV 5	614
8	4,9	HV 5	619
9	5,6	HV 5	628
10	6,3	HV 5	637
11	7	HV 5	617

Row 3:

Indentation	Xdistance[mm]	Method	Hardness[HV5]
1	0	HV 5	595
2	1	HV 5	630
3	2	HV 5	612
4	3	HV 5	612
5	4	HV 5	628
6	5	HV 5	628
7	6	HV 5	633
8	7	HV 5	637

Sintered WC/Co X1:

Row 1:

Indentation	Xdistance[mm]	Method	Hardness[HV5]
1	0,3	HV 5	998
2	1,1	HV 5	1001
3	1,9	HV 5	988
4	2,7	HV 5	1026
5	3,5	HV 5	971
6	4,3	HV 5	997
7	5,1	HV 5	966
8	5,9	HV 5	975
9	6,7	HV 5	1002

Row 2:

Indentation	Xdistance[mm]	Method	Hardness[HV5]
1	0,3	HV 5	980
2	1	HV 5	984
3	1,7	HV 5	984
4	2,4	HV 5	993
5	3,1	HV 5	984
6	3,8	HV 5	984
7	4,5	HV 5	980
8	5,2	HV 5	998
9	5,9	HV 5	980
10	6,6	HV 5	993
11	7,3	HV 5	989
12	8	HV 5	1012

Row 3:

Indentation	Xdistance[mm]	Method	Hardness[HV5]
1	0,3	HV 5	975
2	1	HV 5	975
3	1,7	HV 5	989
4	2,4	HV 5	975
5	3,1	HV 5	984
6	3,8	HV 5	998
7	4,5	HV 5	998
8	5,2	HV 5	966
9	5,9	HV 5	989
10	6,6	HV 5	984
11	7,3	HV 5	998
12	8	HV 5	1012

Sintered WC/Co X2:

Row 1:

Indentation	Xdistance[mm]	Method	Hardness[HV5]
1	0,3	HV 5	1597
2	1	HV 5	1607
3	1,7	HV 5	1588
4	2,4	HV 5	1607
5	3,1	HV 5	1616
6	3,8	HV 5	1616
7	4,5	HV 5	1616
8	5,2	HV 5	1635
9	5,9	HV 5	1664
10	6,6	HV 5	1616
11	7,3	HV 5	1579
12	8	HV 5	1607

Row 2:

Indentation	Xdistance[mm]	Method	Hardness[HV5]
1	0,3	HV 5	1552
2	1	HV 5	1561
3	1,7	HV 5	1616
4	2,4	HV 5	1588
5	3,1	HV 5	1552
6	3,8	HV 5	1561
7	4,5	HV 5	1570
8	5,2	HV 5	1579
9	5,9	HV 5	1570
10	6,6	HV 5	1570
11	7,3	HV 5	1635

Row 3:

Indentation	Xdistance[mm]	Method	Hardness[HV5]
1	0,3	HV 5	1552
2	1	HV 5	1588
3	1,7	HV 5	1570
4	2,4	HV 5	1579
5	3,1	HV 5	1570
6	3,8	HV 5	1597
7	4,5	HV 5	1588
8	5,2	HV 5	1626
9	5,9	HV 5	1635
10	6,6	HV 5	1645
11	7,3	HV 5	1626
12	8	HV 5	1626

C

Appendix C

Here you can find the particle size distribution(PSD) of all the conducted tests. P80 table used for measuring the particle size in each step of the whole test can be seen as well for each test.

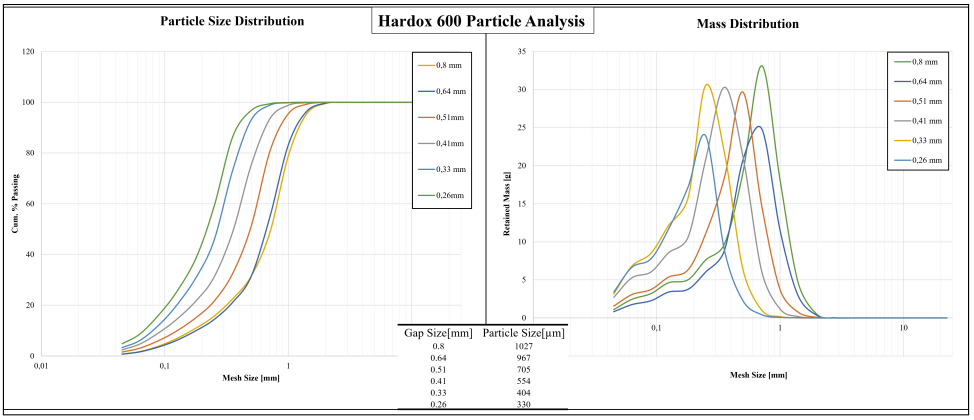

Figure C.1: PSD of Hardox600

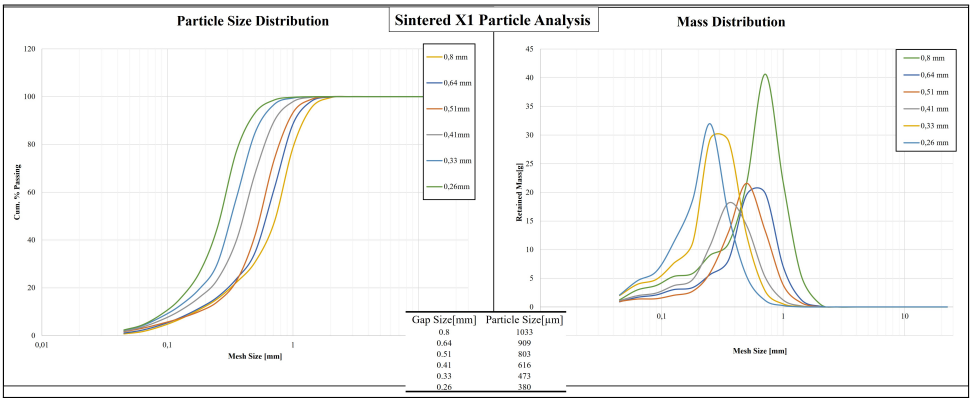

Figure C.2: PSD of Sintered WC/Co X1

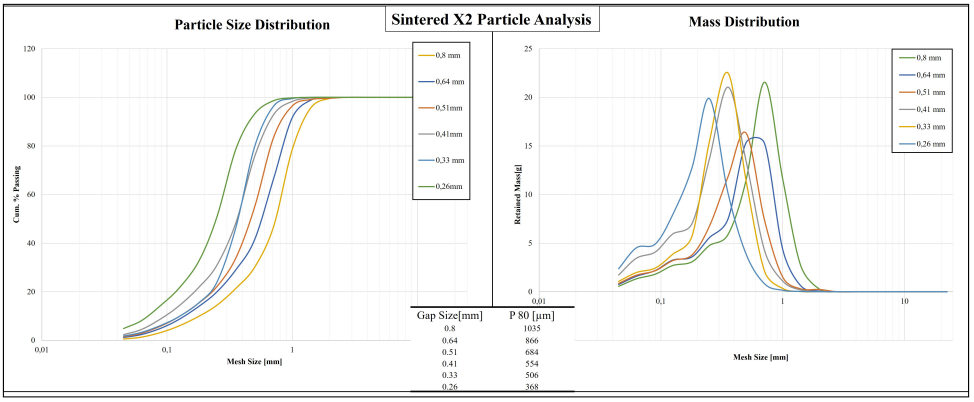

Figure C.3: PSD of Sintered WC/Co X2

DEPARTMENT OF MATERIALS ENGINEERING
CHALMERS UNIVERSITY OF TECHNOLOGY
Gothenburg, Sweden
www.chalmers.se

CHALMERS
UNIVERSITY OF TECHNOLOGY